

EFFECT OF RICE STRAW LOADING ON MORPHOLOGICAL, THERMAL, GAS BARRIER, AND
MECHANICAL PROPERTIES OF POLY(LACTIC ACID)/POLY(3-HYDROXYBUTYRATE-CO-4-
HYDROXYBUTYRATE) BLEND FILMS



A Thesis Submitted in Partial Fulfillment of the Requirements
for the Degree of Master of Engineering in Chemical Engineering
Department of Chemical Engineering
Faculty Of Engineering
Chulalongkorn University
Academic Year 2023

ผลกระทบของปริมาณฟางข้าวที่มีผลต่อสมบัติทางสัณฐานวิทยา ทางความร้อน การซึมผ่านของก๊าซ และทางกล ของฟิล์มพอลิเมอร์ผสมระหว่างพอลิแลคติกแอซิด และพอลิ(3-ไฮดรอกซีบิวทิเรต-โค-4-ไฮดรอกซีบิวทิเรต)



วิทยานิพนธ์นี้เป็นส่วนหนึ่งของการศึกษาตามหลักสูตรปริญญาวิศวกรรมศาสตรมหาบัณฑิต
สาขาวิชาวิศวกรรมเคมี ภาควิชาวิศวกรรมเคมี
คณะวิศวกรรมศาสตร์ จุฬาลงกรณ์มหาวิทยาลัย
ปีการศึกษา 2566

6472028021 : MAJOR CHEMICAL ENGINEERING

KEYWORD: Polylactic acid, Poly(3-hydroxybutyrate-co-4-hydroxybutyrate), Rice straw, Polymer blend, Polymer composite

Danaipat Tuangwattanasin : EFFECT OF RICE STRAW LOADING ON MORPHOLOGICAL, THERMAL, GAS BARRIER, AND MECHANICAL PROPERTIES OF POLY(LACTIC ACID)/POLY(3-HYDROXYBUTYRATE-CO-4-HYDROXYBUTYRATE) BLEND FILMS. Advisor: Prof. ANONGNAT SOMWANGTHANAROJ, Ph.D.

This research focuses on enhancing the properties of polylactic acid (PLA), a biodegradable polymer known for its potential in mitigating waste accumulation issues. The inherent brittleness of PLA poses a significant challenge. To overcome this limitation, the study explores the incorporation of the biodegradable polymer poly(3-hydroxybutyrate-co-4-hydroxybutyrate) (P3HB4HB) into PLA. The PLA/P3HB4HB blend films were prepared by varying compositions from 100/0 to 60/40 wt/wt and using compression molding. The investigations indicated that the PLA/P3HB4HB 90/10 blend film exhibits superior properties, such as synergistic toughness and increased %strain. Rice straw (RS) fiber is introduced as a reinforcing fiber in the blends, expanding the study to the development of PLA/P3HB4HB/RS composite films. These composite films were created by incorporating 3, 5, and 7 phr of untreated RS fiber and compared the influences of untreated RS fiber with alkaline treated RS fiber. Consequently, the treated RS fiber demonstrates higher interfacial adhesion between RS fiber and polymer matrix, leading to improvements in mechanical and gas barrier properties. Furthermore, the treated RS fiber yields a higher %crystallinity in the composite compared to the untreated RS fiber.

Field of Study: Chemical Engineering

Student's Signature

Academic Year: 2023

Advisor's Signature

ACKNOWLEDGEMENTS

This thesis project can be accomplished by supporting the research project from the research fund of Professor Anongnat Somwangthanaroj, thesis advisor. I would like to express my sincere thanks to my advisor for valuable advice and continuous support during my Master's Degree study and this research.

I would like to express my sincere thanks to Mr. Krittapas Charoensuk and everyone in the Polymer Engineering Research Laboratory, Department of Chemical Engineering, Chulalongkorn University, for suggestions, assistance, discussions, friendly encouragement, and for solving various problems.

Finally, I most gratefully acknowledge my family for all their support throughout the period of this research.

Danaipat Tuangwattanasin



TABLE OF CONTENTS

	Page
.....	iii
ABSTRACT (THAI).....	iii
.....	iv
ABSTRACT (ENGLISH).....	iv
ACKNOWLEDGEMENTS.....	v
TABLE OF CONTENTS.....	vi
LIST OF TABLES.....	1
LIST OF FIGURES.....	2
Chapter 1 Introduction.....	5
1.1 General introduction.....	5
1.2 Objective.....	6
1.3 Scopes.....	6
1.4 Research plan.....	7
Chapter 2 Theory and Literature review.....	8
2.1 Polylactic acid (PLA).....	8
2.2 Poly(3-hydroxybutyrate-co-4-hydroxybutyrate) (P3HB4HB).....	8
2.3 Rice straw (RS).....	9
2.4 Alkaline pretreatment of rice straw.....	10
2.5 The effect of polymer blending on morphological properties.....	11
2.6 The effect of polymer blending on thermal properties.....	14
2.7 The effect of polymer blending on gas barrier properties.....	18

2.8 The effect of polymer blending on mechanical properties.....	20
2.9 The effect of rice straw on properties of polymer blends.....	22
Chapter 3 Experiments	32
3.1 Materials.....	32
3.2 Preparation of rice straw fiber (RS)	32
3.3 Characterization of rice straw fiber (RS).....	32
3.3.1 The chemical structures.....	32
3.3.2 The morphological properties.....	32
3.3.3 The thermal stability.....	33
3.4 Preparation of PLA/P3HB4HB blend films and PLA/P3HB4HB/RS composite films	33
3.5 Characterization of PLA/P3HB4HB blend and PLA/P3HB4HB/RS composite films	34
3.5.1 The morphological properties.....	34
3.5.2 The thermal properties	35
3.5.3 The gas barrier properties.....	35
3.5.4 The mechanical properties.....	36
Chapter 4 Results and Discussion	37
4.1 Characterization of rice straw fiber (RS).....	37
4.1.1 The chemical structures.....	37
4.1.2 The morphological properties.....	38
4.1.3 The thermal stability.....	38
4.2 Characterization of PLA/P3HB4HB blend films	39
4.2.1 The morphological properties.....	39

4.2.2 The thermal properties	40
4.2.3 The gas barrier properties	42
4.2.4 The mechanical properties.....	44
4.3 Characterization of PLA/P3HB4HB/RS composite films.....	46
4.3.1 The morphologies properties.....	46
4.3.2 The crystalline formation in PLA/P3HB4HB blend and PLA/P3HB4HB/RS composites.....	47
4.3.3 The thermal properties	48
4.3.4 The gas barrier properties	49
4.3.5 The mechanical properties.....	51
Chapter 5 Conclusions.....	53
REFERENCES	54
VITA.....	58

LIST OF TABLES

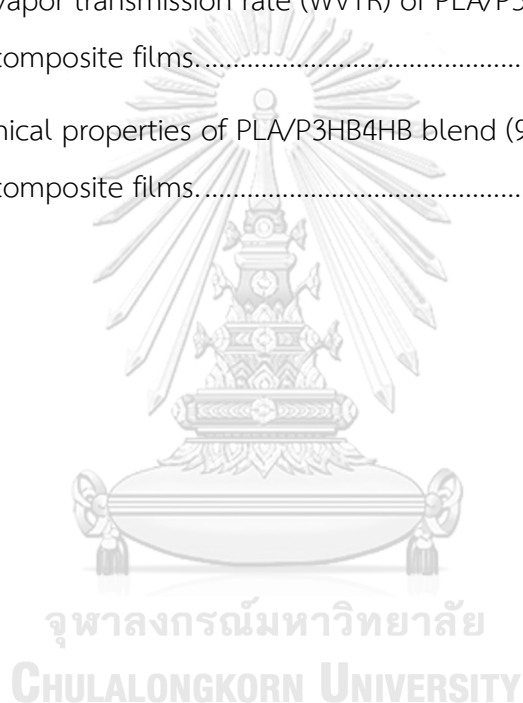
	Page
Table 1.1 Research implementation timeline.	7
Table 2.1 Thermal properties of PLA/P3HB4HB cast films at first heating cycle [3]	15
Table 2.2 Thermal properties of PHBV/PLA blends [12].	17
Table 2.3 Thermal properties of PLA/PBS/SB and PLA/PBS/NPCC composites [13]. ...	18
Table 2.4 Barrier properties of PLA/P3HB4HB blends [3].	18
Table 2.5 The mechanical properties of PLA/P3HB4HB blends in MD [3].	21
Table 2.6 The mechanical properties of PHB/P3HB4HB blends [14].	22
Table 2.7 Thermal properties of polymer composites [16].	26
Table 2.8 Mechanical properties of polymer composites [16].	28
Table 2.9 Thermal properties of unmodified PLA and each of the three treatments [11].	30
Table 3.1 Composition of PLA/P3HB4HB blends	33
Table 3.2 Composition of PLA/P3HB4HB/RS composites	34
Table 4.1 Thermal properties of PLA/P3HB4HB blend films.	42
Table 4.2 Mechanical properties of PLA/P3HB4HB blend films.	45
Table 4.3 Thermal properties of PLA/P3HB4HB blend (90/10) and PLA/P3HB4HB/RS composite films.	49
Table 4.4 Mechanical properties of PLA/P3HB4HB blend (90/10) and PLA/P3HB4HB/RS composite films.	52

LIST OF FIGURES

	Page
Figure 2.1 Chemical structure of PLA.	8
Figure 2.2 Chemical structure of P3HB4HB.	9
Figure 2.3 Chemical structure of (A) cellulose, (B) hemicellulose, and (C) lignin [8]. ..	10
Figure 2.4 The effect of alkaline pretreatment on the structure of lignocellulosic biomass [10].	11
Figure 2.5 Cross-sectional SEM images of the P3HB4HB/PLA blends with decreasing P3HB4HB content from (a) 50, (b) 45, (c) 40, (d) 35, and (e) 30 wt%, respectively [7].	12
Figure 2.6 Cross-sectional SEM images of the (a) pure PHBV, (b) pure PLA, and PHBV/PLA blends with increasing PLA content from (c) 25, (50), and (75) wt%, respectively [12].	13
Figure 2.7 The polarized optical microscopy of (a) pure PLA and PLA/HBNA blends with increasing HBNA from (b) 0.50, (c) 0.75, and (d) 1.00 wt%, respectively at 135 °C [6].	14
Figure 2.8 DSC thermograms of PLA/P3HB4HB blends at first heating cycle [3].	15
Figure 2.9 DSC thermograms of PHBV/PLA blends at second heating cycle [12].	16
Figure 2.10 DSC thermograms of PHBV/PLA blends at cooling cycle [12].	17
Figure 2.11 The oxygen permeability of PHBV/PLA blends [12].	19
Figure 2.12 The water vapor permeability of PHBV/PLA blends [12].	20
Figure 2.13 The stress-strain curves of PLA/P3HB4HB blends in MD [3].	21
Figure 2.14 The stress-strain curves of PHB/P3HB4HB blends [14].	22
Figure 2.15 Physical properties of polymer composite films with RS content from (a) 3, (b) 5, and (c) 10 wt%, respectively [15].	23
Figure 2.16 Morphological properties of (a) pure PLA and (b) PLA/NR (70/30 wt%) with increasing RS content from (c) 3, (d) 5, and (e) 10 wt%, respectively [15].	24

Figure 2.17 Mechanical properties of pure PLA and PLA/NR (70/30 wt%) with increasing RS content from 3, 5, and 10 wt%, stress-strain curves (a) machine direction, (b) transverse direction, (c) Young's modulus, (d) tensile strength, and (e) elongation at break [15].	25
Figure 2.18 DSC thermograms of polymer composites [16].	26
Figure 2.19 Cross-sectional SEM images of (a) pure PLA with fixed amounts of RSS (10 wt%) and vary the size of RSS (b) PLA/10.0/S, (c) PLA/10.0/M, and (d) PLA/10.0/L [16].	27
Figure 2.20 SEM images of PLA/RS composite films (a) unmodified, (b) NaOH, (c) KBM403, and (d) TEOS treatments [11].	29
Figure 2.21 DSC thermograms of unmodified PLA and each of the three treatments [11].	30
Figure 4.1 FT-IR spectra of untreated and treated rice straw fiber.	37
Figure 4.2 FE-SEM images of (a) untreated and (b) treated rice straw fiber at 150 magnification.	38
Figure 4.3 TGA and DTG curves of untreated and treated rice straw fiber.	39
Figure 4.4 Cross-sectional FE-SEM images of (a) pure PLA, PLA/P3HB4HB blends: (b) 90/10, (c) 80/20, (d) 70/30, (e) 60/40, and (f) pure P3HB4HB at 3000 magnification.	40
Figure 4.5 DSC thermograms of PLA/P3HB4HB blend films.	41
Figure 4.6 Oxygen transmission rate (OTR) of PLA/P3HB4HB blend films.	43
Figure 4.7 Water vapor transmission rate (WVTR) of PLA/P3HB4HB blend films.	44
Figure 4.8 Mechanical properties of PLA/P3HB4HB blend films.	45
Figure 4.9 Cross-sectional FE-SEM images of (a) PLA/P3HB4HB blend, PLA/P3HB4HB/RS composites: (b) 90/10/3 untreated, (c) 90/10/5 untreated, (d) 90/10/7 untreated, and (e) 90/10/3 treated at 3000 magnification.	46

Figure 4.10 POM images of (a) PLA/P3HB4HB blend (90/10) and composites filled with untreated RS (b) 3 wt%, (c) 5 wt%, and (d) treated RS 3wt% at 120 °C, for a duration of = (a0, b0, c0, d0) 0 min, (a1, b1, c1, d1) 2 mins, and (a2, b2, c2, d2) 5 mins.....	47
Figure 4.11 DSC thermograms of PLA/P3HB4HB blend (90/10) and PLA/P3HB4HB/RS composite films.	48
Figure 4.12 Oxygen transmission rate (OTR) of PLA/P3HB4HB blend (90/10) and PLA/P3HB4HB/RS composite films.....	50
Figure 4.13 Water vapor transmission rate (WVTR) of PLA/P3HB4HB blend (90/10) and PLA/P3HB4HB/RS composite films.....	51
Figure 4.14 Mechanical properties of PLA/P3HB4HB blend (90/10) and PLA/P3HB4HB/RS composite films.....	52



Chapter 1

Introduction

1.1 General introduction

Currently, polymers derived from petroleum are widely used in industries including agriculture and packaging. These polymers exhibit excellent attributes for their applications, are cost-effective, and have durability. However, they do not have biodegradable properties, which contributes to the issue of waste accumulation in the environment. Consequently, the use of biodegradable polymers that have biodegradable properties has the potential to reduce the issue of waste accumulation [1].

The biodegradable polymers are environmentally friendly, have biodegradability, and are biocompatible. Polylactic acid (PLA) is one of the biodegradable polymers that is derived from renewable sources such as corn, potatoes, and cassava. PLA has excellent biodegradability, transparency, and mechanical strength. However, its brittleness is the main drawback of PLA, which makes it an issue for extensive applications. Other drawbacks include gas permeability and thermal instability [2]. Therefore, combining PLA with other biodegradable polymers to improve its drawbacks is an alternative.

Polyhydroxyalkanoates (PHA) are bio-polyesters produced by microorganisms. Poly(3-hydroxybutyrate-co-4-hydroxybutyrate) (P3HB4HB) is a known PHA member and is produced from copolymerization between poly(3-hydroxybutyrate) (P3HB) and 4-hydroxybutyrate (4HB). P3HB4HB is interesting because it has a wide range of physical, thermal, and mechanical properties depending on the amount of 4HB. Increasing the amount of 4HB exhibits a change in properties from semi-crystalline (rigid) to amorphous (flexible) and decreased in melting temperature [3]. P3HB4HB with a high amount of 4HB has biodegradability, is biocompatible, and has excellent flexural strength.

PLA and P3HB4HB have a slow crystallization behavior, which impacts their properties and applications. Adding nucleating agents, which operate as heterogeneous nuclei and accelerate the crystallization process of polymers, is the

most extensively used technique for improving polymer crystallization behavior. In addition, the thermal and mechanical properties of polymers can be enhanced by higher crystallinity [4].

Rice straw (RS) derived from renewable sources (agricultural waste) was chosen. RS can act as a nucleating agent in the polymer matrix [5] and has the potential to enhance the biodegradability, thermal, and mechanical properties of the polymeric matrix for composite materials. In addition, the use of RS can reduce the environmental impact because the combustion of RS produces carbon dioxide (CO₂) and particulate matter (PM).

This research is focused on the development of PLA/P3HB4HB blend films. After the optimal ratio of PLA/P3HB4HB blend is achieved, RS will be mixed with the blend to study the effect of RS loading on the morphological, thermal, gas barrier, and mechanical properties of PLA/P3HB4HB/RS composite films by means of reinforcing and nucleating effects.

1.2 Objective

To investigate the effect of RS loading on morphological, thermal, gas barrier, and mechanical properties of PLA/P3HB4HB blend films.

1.3 Scopes

1.3.1 PLA/P3HB4HB was blended with weight ratios of 100/0, 90/10, 80/20, 70/30, and 60/40 are mixed.

1.3.2 After mixing different weight ratios, the best condition was chosen to mix with RS (3, 5, and 7 wt%).

1.3.3 Morphological, thermal, gas barrier, and mechanical properties of PLA/P3HB4HB blend and PLA/P3HB4HB/RS composite films were studied.

1.4 Research plan

Table 1.1 Research implementation timeline.

Activities	Period									
	2023									
	Jan	Feb	Mar	Apr	May	Aug	Sep	Oct	Nov	Dec
1. Research and literature reviews were studied.										
2. PLA/P3HB4HB blend and PLA/P3HB4HB/RS composite films were prepared.										
3. The characteristics of PLA/P3HB4HB blend and PLA/P3HB4HB/RS composite films were analyzer.										
4. The experiment results were analyzed.										
5. Write a thesis										

Chapter 2

Theory and Literature review

2.1 Polylactic acid (PLA)

PLA is a biodegradable polymer that is derived from renewable sources such as corn, potatoes, and cassava. PLA is a biodegradable and biocompatible linear aliphatic thermoplastic polyester that can be used as an alternative to petroleum based polymers [2]. PLA has exceptional properties such as tensile strength and transparency that make it suitable for applications such as food packaging and agricultural fields. However, PLA is brittle, which is the main drawback, and other drawbacks include thermal instability and slow crystallization behavior during molding processes involving extrusion and injection, which influence the percentage of crystallinity of PLA and barrier properties [1, 6]. The chemical structure of PLA is shown in Figure 2.1.

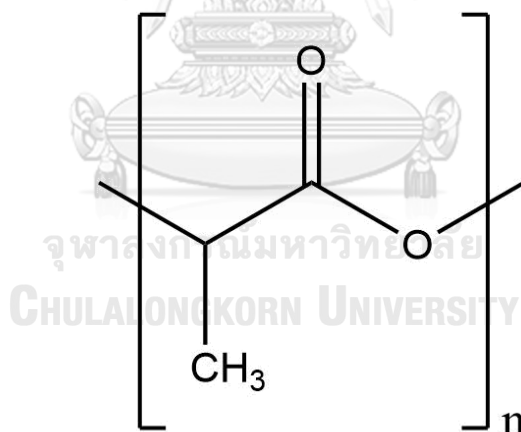


Figure 2.1 Chemical structure of PLA.

2.2 Poly(3-hydroxybutyrate-co-4-hydroxybutyrate) (P3HB4HB)

Polyhydroxyalkanoates (PHA) are bio-polyesters produced by various microorganisms as intracellular carbon and energy storage [7]. They are non-toxic, completely biodegradable, and biocompatible. Poly(3-hydroxybutyrate) (P3HB) is a member of PHA. Due to its high crystallinity and brittleness, its applications are limited.

Poly(3-hydroxybutyrate-co-4-hydroxybutyrate) (P3HB4HB) is a new generation of PHA created by copolymerizing P3HB and 4-hydroxybutyrate (4HB). P3HB4HB is interesting because its physical, thermal, and mechanical properties vary widely depending on the amount of 4HB. Increasing the amount of 4HB results in a transition from semi-crystalline (rigid) to amorphous (flexible) properties and a decrease in melting temperature. P3HB4HB exhibits semi-crystalline plastic behavior with less than 10 mol% of 4HB or completely amorphous elastomer behavior with more than 40 mol% of 4HB [3]. The amount of 4HB influences the crystallization behavior of P3HB4HB, resulting in slow crystallization and a low percentage of crystallinity, which affect the physical, thermal, barrier, and mechanical properties of P3HB4HB [4]. The chemical structure of P3HB4HB is shown in Figure 2.2.

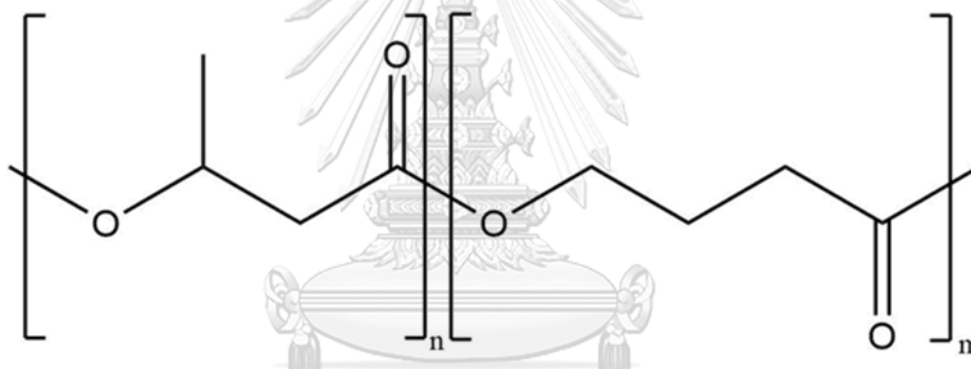


Figure 2.2 Chemical structure of P3HB4HB.

2.3 Rice straw (RS)

Rice straw (RS), which is derived from agricultural waste, is a sustainable energy source for society as it contains lignocellulosic biomass and has the capacity to generate enormous amounts of energy [8]. Carbon dioxide (CO₂) and particulate matter (PM) are byproducts of the combustion of RS, which has a negative impact on the environment. Rice straw is produced in large quantities and generates waste.

Lignocellulosic biomass from RS, which containing cellulose (31.1%), hemicellulose (22.3%), lignin (13.3%), and other components (33.3%) [8]. Cellulose is a polysaccharide and the primary component of lignocellulosic biomass, which provides fiber strength. Cellulose fibrils are formed by hydrogen and Vander Waals

bonds connecting the cellulosic chain. Hemicelluloses are comprised of distinct sugar units, exhibit less polymerization, and are hydrolysable. Lignin that is an aromatic polymer, containing syringyl, guaiacyl, and p-hydroxy phenol are associated together to the cross-linked structure [9, 10]. The chemical structure of cellulose, hemicellulose, and lignin are shown in Figure 2.3.

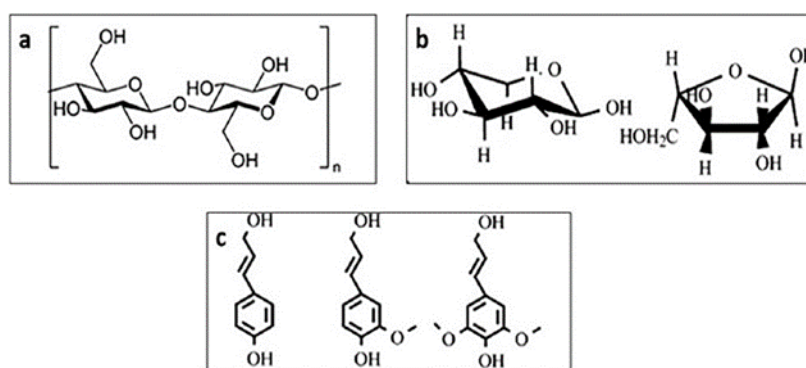


Figure 2.3 Chemical structure of (A) cellulose, (B) hemicellulose, and (C) lignin [8].

2.4 Alkaline pretreatment of rice straw

Rice straw (RS) is a lignocellulosic biomass that is composed of cellulose, hemicellulose, and lignin. Polarity and moisture absorption have hydrophilic properties of these components. The majority of biodegradable polymers have hydrophobic properties. When RS is combined with these polymers, there is poor interfacial adhesion. Pretreatment is an option for enhancing the interfacial adhesion between RS and biodegradable polymers, which modifies the surface roughness, and reduces the moisture absorption as well as other properties of composites [10, 11].

Alkaline pretreatment is one of several effective strategies for modifying the structure of lignocellulosic biomass. This method increases the surface roughness, resulting in improved interfacial adhesion between RS and biodegradable polymers, which enhances the compatibility of composites. When breaking the lignocellulosic structure into smaller fibrils, the surface area of RS is increased. Alkali treatment modifies the chemical structure of RS by decomposing hemicellulose and lignin, thereby increasing the surface area for interaction with the polymer matrix and enhancing wettability. NaOH is commonly used as an alkali pretreatment for RS, and

the concentration of NaOH has an effect on the hydrolysable of hemicellulose and lignin [10, 11]. The effect of alkaline pretreatment shown in Figure 2.4.

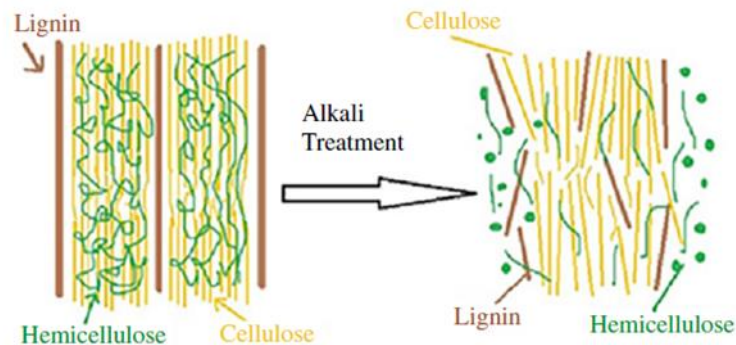


Figure 2.4 The effect of alkaline pretreatment on the structure of lignocellulosic biomass [10].

2.5 The effect of polymer blending on morphological properties

Chen et al. (2020) [7] investigated the melt spinning and hot drawing of P3HB4HB/PLA blends, with P3HB4HB exhibiting semi-crystalline behavior and a 4HB content of 11 mol%. The morphological properties of the polymer blends, as shown in Figure 2.5, when the amount of P3HB4HB was (a) 50 and (b) 45 wt%, revealed a smooth surface and brittle fracture behavior. However, the amount of P3HB4HB was less than (c, d, and e) 40 wt% and exhibited a rough surface and ductile fracture behavior. As a result of a decrease in the amount of P3HB4HB, the morphology of polymer blends changed from the co-continuous phase to the sea-island phase. The appearance of phase separation demonstrated the immiscibility of polymer blends.

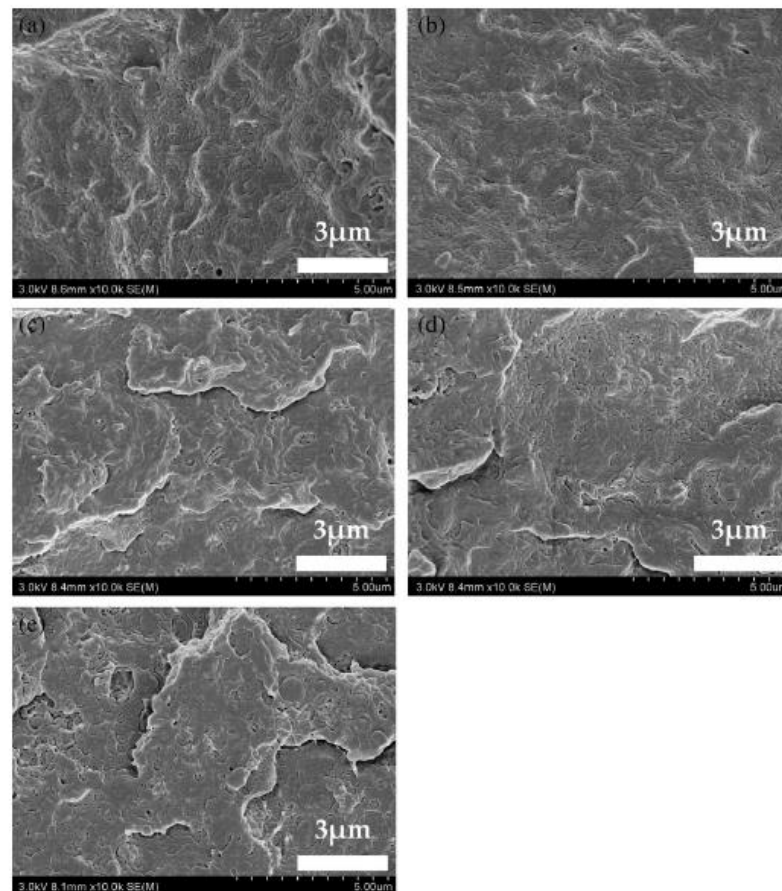


Figure 2.5 Cross-sectional SEM images of the P3HB4HB/PLA blends with decreasing P3HB4HB content from (a) 50, (b) 45, (c) 40, (d) 35, and (e) 30 wt%, respectively [7].

Zembouai, Kaci, et al. (2013) [12] investigated poly(3-hydroxybutyrate-co-3-hydroxyvalerate) (PHBV) with PLA blends prepared by melt mixing, after that, films were prepared by compression molding. The morphological properties of the polymer blends, as shown in Figure 2.6, The disorganized fracture showed in (a) the pure PHBV because of its crystalline form. The organized fracture showed in (b) the pure PLA because of its amorphous form and contained holes affected by processing. With increasing PLA content from (c) 75, (d) 50, and (e) 25 wt%, respectively. The appearance of phase separation was shown in all conditions and exhibited a rough surface on polymer blends. When less than polymer content acted as inclusion (beads) and not regular distribution in polymer blends. The co-continuous phase was identified when the content of both polymers was identical.

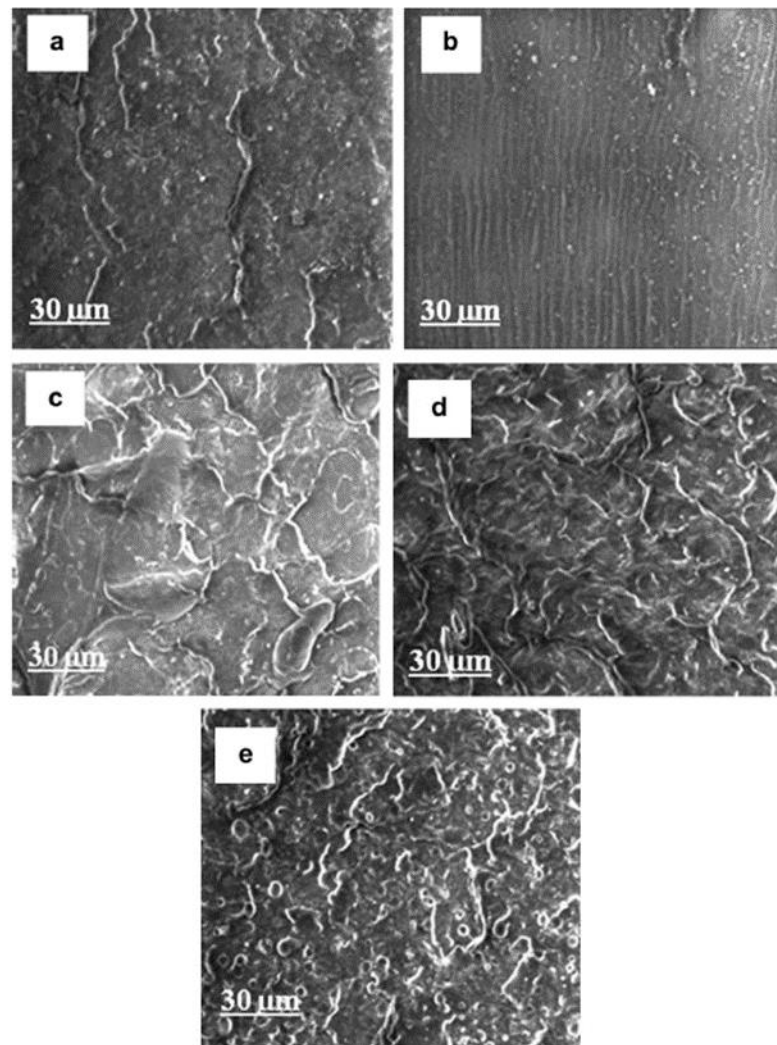


Figure 2.6 Cross-sectional SEM images of the (a) pure PHBV, (b) pure PLA, and PHBV/PLA blends with increasing PLA content from (c) 25, (50), and (75) wt%, respectively [12].

Niu et al. (2023) [6] investigated PLA with (N'-(3-(hydraziny-loxy) benzoyl)-1-naphthohydrazide) (HBNA) as nucleating agent and blending by melt mixing, after which compression molded films were created. The morphology of the crystallization behavior of polymer blends at 135 °C, as shown in Figure 2.7, (a) pure PLA exhibited a low nuclei density and crystallization rate. The addition of HBNA resulted in increased nuclei density, decreased size of the crystal, a rapid crystallization rate that led to the formation of a complete crystal within 2 minutes (0.75 and 1 wt% of HBNA), and enhanced crystallinity of PLA.

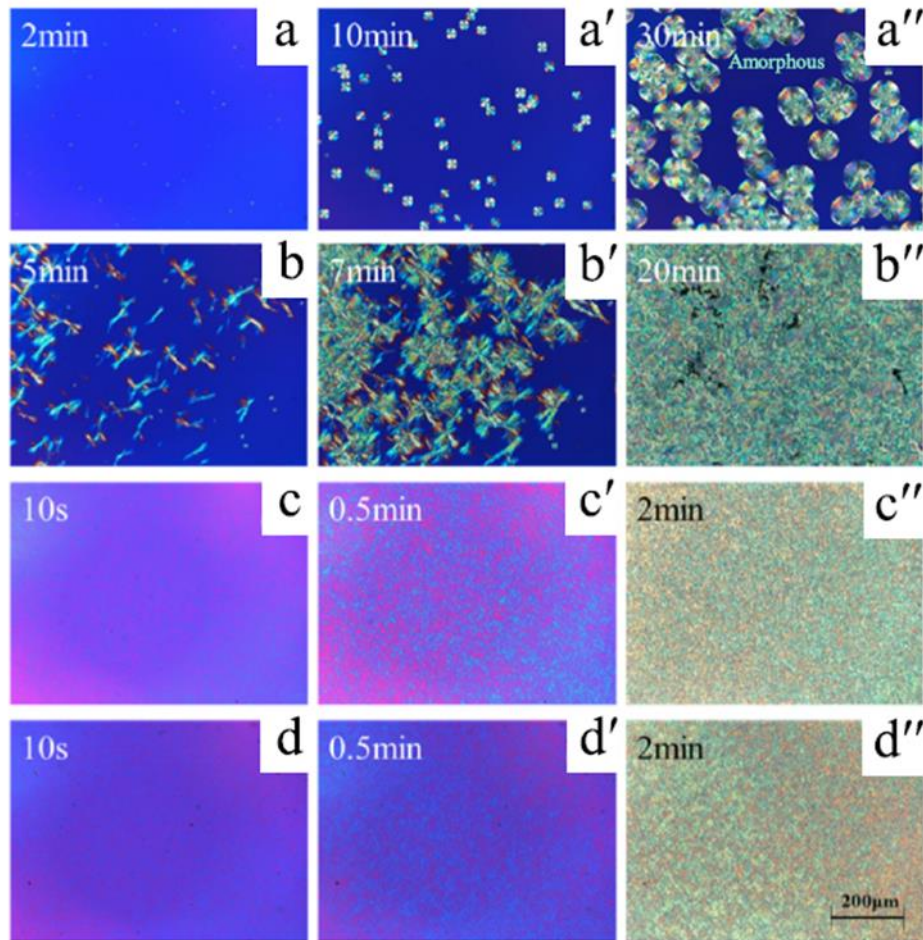


Figure 2.7 The polarized optical microscopy of (a) pure PLA and PLA/HBNA blends with increasing HBNA from (b) 0.50, (c) 0.75, and (d) 1.00 wt%, respectively at 135 °C [6].

2.6 The effect of polymer blending on thermal properties

Aversa et al. (2023) [3] investigated PLA/P3HB4HB blends produced by casting films containing P3HB4HB amorphous phase. The thermal properties of the polymer blends, as shown in Figure 2.8 and Table 2.1, resulted in the glass transition temperature (T_g) of P3HB4HB being approximately -17 °C and decreasing with increasing P3HB4HB content. The T_g of PLA decreased from 73 to 61 °C, indicating that the molecular chain of PLA unfroze and movement occurred from the amorphous phase of P3HB4HB. The melting temperature (T_m) of P3HB4HB was approximately 80 °C and the presence of multiple peaks confirmed that P3HB4HB

consists mainly of the amorphous phase. The T_m of PLA is not significantly decreased with increasing P3HB4HB and has a double melting peak (P3HB4HB 20 wt% or CL20), indicating that it has unstable crystalline phases of PLA. The cold crystallization temperature (T_{cc}) of PLA decreased from 81 to 77 °C with increasing P3HB4HB content, indicating that P3HB4HB acts as a nucleating agent in the PLA matrix. When P3HB4HB content increased, the percentage of crystallinity (X_c) increased, confirming that P3HB4HB produced a heterogeneous phase in the PLA matrix. The excess of P3HB4HB (limited to P3HB4HB 30 wt% or CL30) hindered cold crystallization and rearrangement of the PLA chain into a crystal, which decreased the percentage of crystallinity.

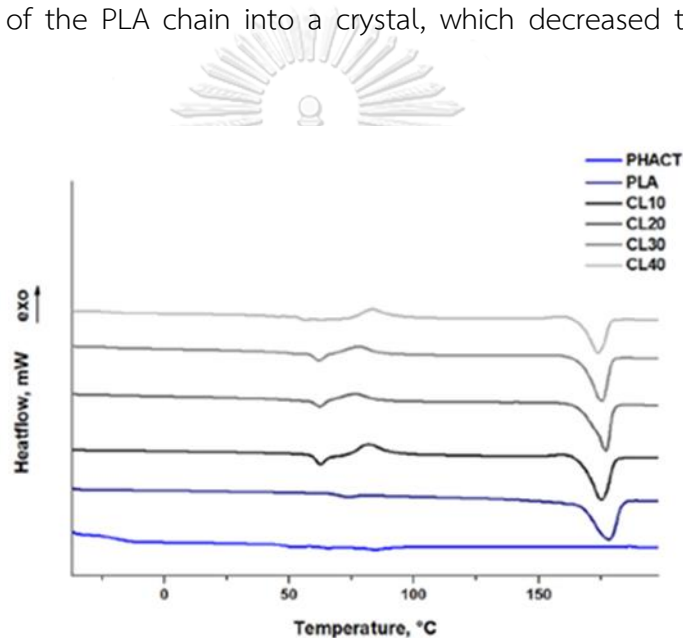


Figure 2.8 DSC thermograms of PLA/P3HB4HB blends at first heating cycle [3].

Table 2.1 Thermal properties of PLA/P3HB4HB cast films at first heating cycle [3]

Polymer	T_g P3HB4HB (°C)	T_g PLA (°C)	T_{cc} PLA (°C)	T_m PLA (°C)	X_c PLA (%)
PLA	N/A	73.28	N/A	176.27	N/A
P3HB4HB	-17.13	N/A	N/A	N/A	N/A
PLA/P3HB4HB (90/10)	N/A	60.14	81.82	174.52	45.44
PLA/P3HB4HB (80/20)	-17.24	61.60	76.42	176.42	48.45
PLA/P3HB4HB (70/30)	-16.05	62.48	77.90	174.59	47.41
PLA/P3HB4HB (60/40)	-18.39	61.58	83.10	173.25	46.37

Zembouai, Kaci, et al. (2013) [12] investigated poly(3-hydroxybutyrate-co-3-hydroxyvalerate) (PHBV) with PLA blends produced by compression molding. The thermal properties of the polymer blends, as shown in Figure 2.9 and Table 2.2, as well as the compatibility between PHBV and PLA were investigated. The glass transition temperature (T_g) of pure PHBV was approximately 3 °C and pure PLA was 59 °C, indicating that the separation of T_g proposed to immiscible blends. The T_g of PLA decreased from 59 to 57 °C, indicating that the amorphous phase increased with increasing PHBV content and increased PLA molecular chain movement.

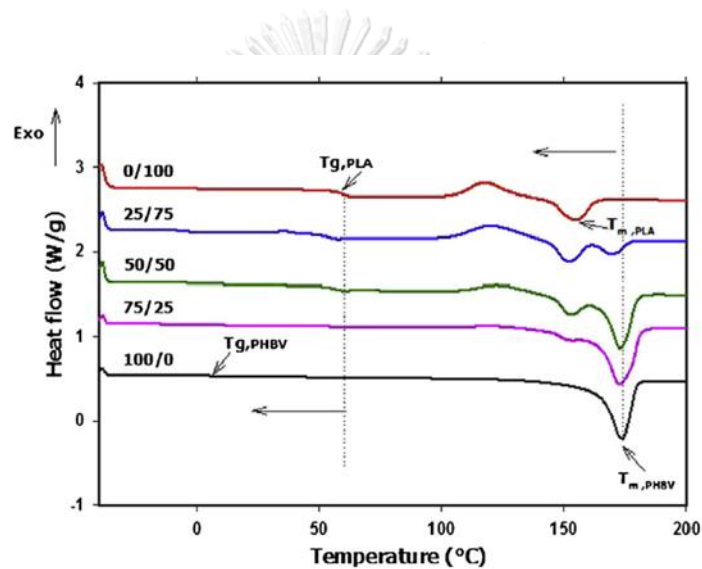


Figure 2.9 DSC thermograms of PHBV/PLA blends at second heating cycle [12].

The crystallization temperature (T_c) of the polymer blends, is shown in Figure 2.10 and Table 2.2, whereas the T_c of pure PLA could not be determined due to insufficient chain crystallization time. The T_c of PHBV decreased as PLA content increased, implying a decrease in nuclei density and an obstacle to the crystallization of PLA in polymer blends. The percentage of crystallinity (X_c) of PHBV decreased with increasing PLA content suggesting that PLA is ineffective as a nucleating agent in polymer blends, in contrast to PHBV [12].

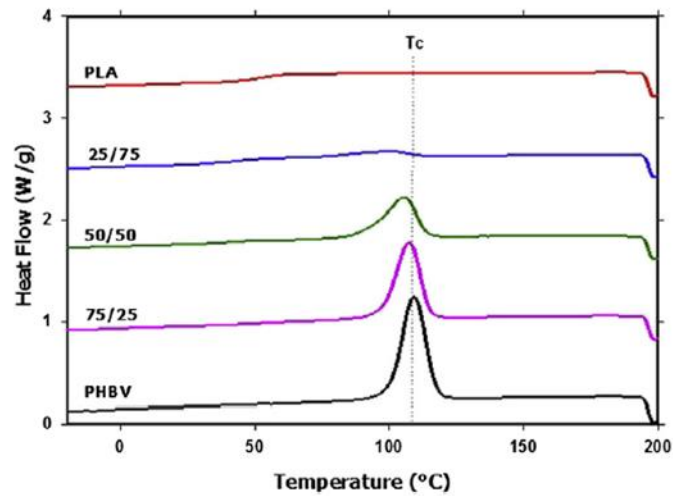


Figure 2.10 DSC thermograms of PHBV/PLA blends at cooling cycle [12]

Table 2.2 Thermal properties of PHBV/PLA blends [12].

Polymer	T_g PLA (°C)	T_g PHBV (°C)	X_c Blend (%)
PHBV/PLA (100/0)	N/A	2.8	47.3
PHBV/PLA (75/25)	57.1	3.0	35.1
PHBV/PLA (50/50)	57.9	3.3	26.2
PHBV/PLA (25/75)	58.4	4.5	7.8
PHBV/PLA (0/100)	59.8	N/A	N/A

Homklin & Hongsriphan (2013) [13] investigated PLA/poly(butylene succinate) (PBS) blends including nucleating agents (sodium benzoate, SB) generated by compression molding, as shown in Table 2.3. The glass transition temperature (T_g) of PLA was not shifted, and PBS was not detected. The crystallization temperature (T_{cc}) of PLA was not established, in contrast to PBS. The addition of SB to polymer blends enhances crystallization in PLA, resulting in a higher percentage of crystallinity (X_c) compared to PBS. SB acted as a nucleating agent, nucleating growth and accelerating the crystallization of PLA.

Table 2.3 Thermal properties of PLA/PBS/SB and PLA/PBS/NPCC composites [13].

Polymer	T _g PLA (°C)	T _g PBS (°C)	T _{cc} PLA (°C)	T _{cc} PBS (°C)	X _c PLA (%)	X _c PBS (%)
PLA/PBS (60/40)	N/A	N/A	N/A	104.10	10.44	62.23
PLA/PBS/SB0.5 (60/40/0.5)	60	N/A	N/A	105.63	21.21	30.23
PLA/PBS/SB1.0 (60/40/1.0)	60	N/A	N/A	106.25	31.95	18.70

2.7 The effect of polymer blending on gas barrier properties

Aversa et al. (2023) [3] investigated PLA/P3HB4HB blends generated by casting films containing P3HB4HB amorphous phase. The gas barrier properties of the polymer blends, as shown in Table 2.4, The oxygen transmission rate (OTR) of polymer blends decreased from 40.59, 22.17, 17.84, and 13.39 cm³/ (m².24h), respectively, with increasing the amount of P3HB4HB. The reason was that the nature of P3HB4HB has lower gas permeation and the effect of nucleation, which enhances gas barrier properties in polymer blends.

The water vapor transmission rate (WVTR) of polymer blends decreased from 9.62, 4.03, 3.41, and 2.93 g/ (m².24h), respectively, with increasing the amount of P3HB4HB. The reasons contributed by the nature of both polymers were hydrophobic properties and an increased percentage of crystallinity, which were previously explained in the effect of polymer blending on thermal properties.

Table 2.4 Barrier properties of PLA/P3HB4HB blends [3].

Polymer	OTR [cm ³ / (m ² .24h)]	WVTR [g/ (m ² .24h)]
PLA/P3HB4HB (90/10)	40.59	9.62
PLA/P3HB4HB (80/20)	22.17	4.03
PLA/P3HB4HB (70/30)	17.84	3.41
PLA/P3HB4HB (60/40)	13.39	2.93

Zembouai, Kaci, et al. (2013) [12] investigated poly(3-hydroxybutyrate-co-3-hydroxyvalerate) (PHBV) with PLA blends generated by compression molding and the thickness of the films was approximately 100-150 μm . The gas barrier properties of the polymer blends, as shown in Figures 2.11 and 2.12, Figure 2.11 shows the oxygen permeability (OP) of polymer blends. The OP of pure PHBV is lower than that of pure PLA, attributed to the semi-crystalline structure of PHBV, as indicated by its oxygen barrier properties. The OP determined the diffusion of gas, which had a significant impact on gas permeation, and gas permeation could only occur through an amorphous phase. Consequently, the increased percentage of crystallinity indicated an increase in the crystalline phase in a polymer, which enhanced its oxygen barrier properties. The increased percentage of crystallinity was previously explained by the effect of polymer blending on thermal properties.

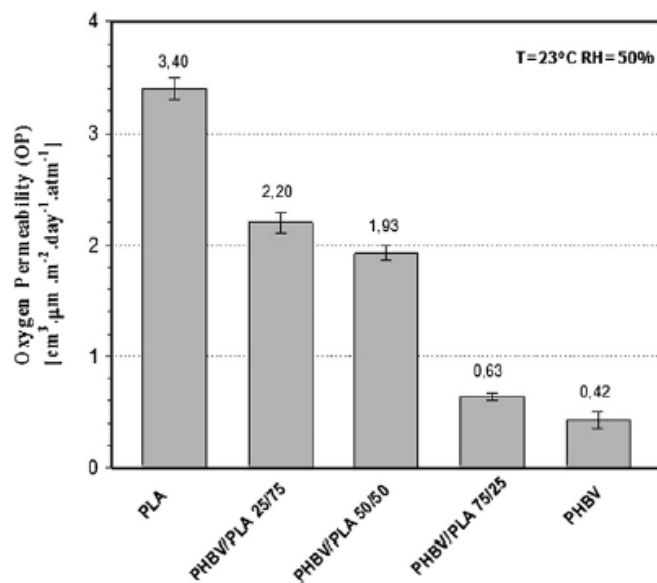


Figure 2.11 The oxygen permeability of PHBV/PLA blends [12].

The water vapor permeability (WVP) of polymer blends is shown in Figure 2.12. The WVP of polymer blends decreased with increasing the amount of PHBV, indicating that PHBV improved the water barrier properties. The enhancement of water barrier properties was attributed to an increase in the amount of crystallinity,

which increased the crystalline phase in polymer blends and prevented the diffusion of gas. In addition, the tortuousness of gas diffusion increased [12].

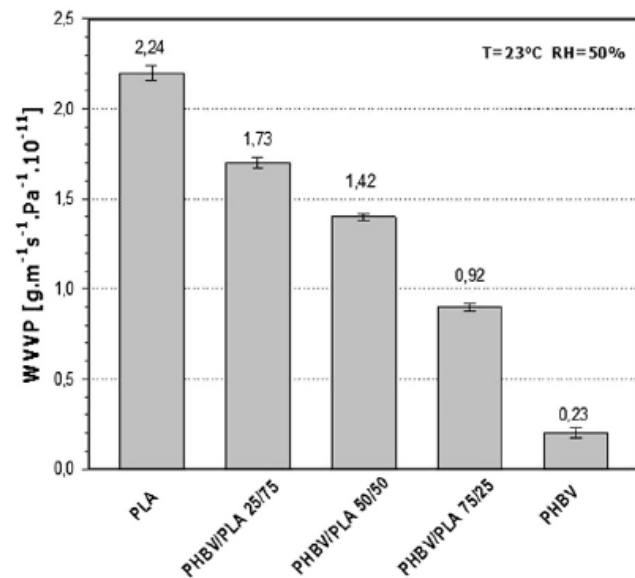


Figure 2.12 The water vapor permeability of PHBV/PLA blends [12].

2.8 The effect of polymer blending on mechanical properties

Aversa et al. (2023) [3] investigated PLA/P3HB4HB blends generated by casting films containing the P3HB4HB amorphous phase. The mechanical properties of the polymer blend along machine direction (MD) are shown in Figure 2.13 and Table 2.5. The stress-strain curves demonstrated that the behavior of polymer blends changed from brittle to ductile and that the elongation at break of polymer blends increased, indicating that the addition of P3HB4HB increased the flexibility of polymer blends. P3HB4HB 40 wt% (CL40) decreased partially, attributing to the complexity of the amount of P3HB4HB greater than 30 wt%. In contrast, the tensile strength and young's modulus decreased.

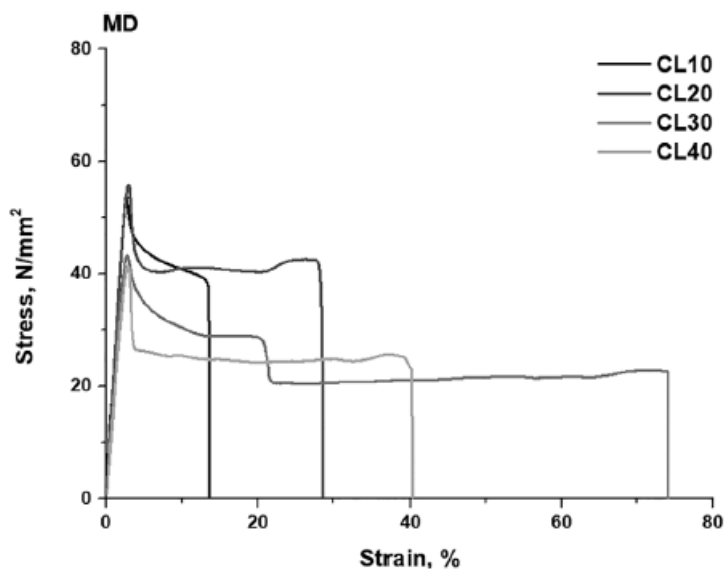


Figure 2.13 The stress-strain curves of PLA/P3HB4HB blends in MD [3].

Table 2.5 The mechanical properties of PLA/P3HB4HB blends in MD [3].

Polymer	Tensile strength (MPa)	Young's modulus (MPa)	Elongation at break (%)
PLA/P3HB4HB (90/10)	42.01 ± 6.19	2483.51 ± 172.36	13.98 ± 4.60
PLA/P3HB4HB (80/20)	47.80 ± 4.34	2451.36 ± 205.98	22.89 ± 7.13
PLA/P3HB4HB (70/30)	35.32 ± 3.16	2100.87 ± 29.60	64.94 ± 11.46
PLA/P3HB4HB (60/40)	21.92 ± 1.81	1885.18 ± 138.60	51.30 ± 8.94

Luo et al. (2007) [14] investigated a poly(3-hydroxybutyrate) (PHB) blend with P3HB4HB generated by solvent casting. P3HB4HB exhibits amorphous behavior and a 4HB content of 41 mol%. The mechanical properties of the polymer blends are shown in Figure 2.14 and Table 2.6. The stress-strain showed that the behavior of polymer blends changed from brittle to ductile at the amount of P3HB4HB greater than 20 wt%, which exhibited ductile behavior. The increased P3HB4HB content had an effect on the tensile strength and young's modulus of polymer blends but increased elongation at break. Pure P3HB4HB was not detected due to the highly amorphous phase, which makes it glue-like, elastic, and unsuitable for this process.

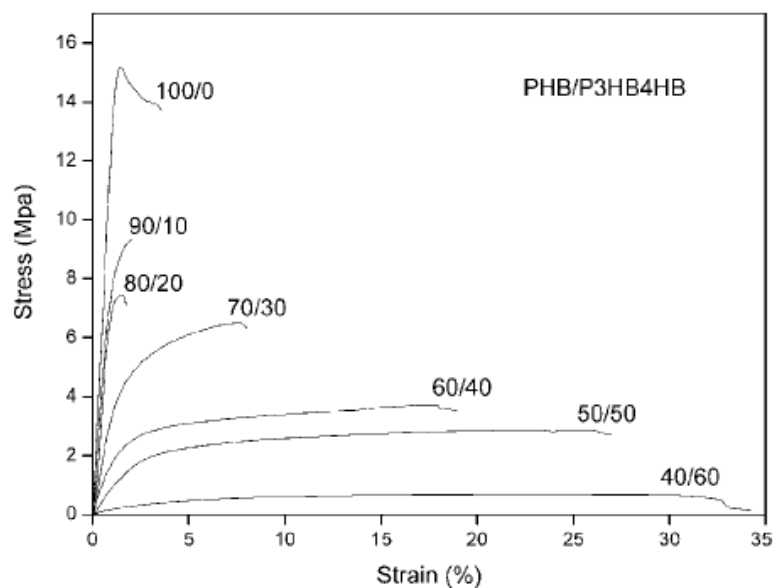


Figure 2.14 The stress-strain curves of PHB/P3HB4HB blends [14].

Table 2.6 The mechanical properties of PHB/P3HB4HB blends [14].

Polymer	Tensile strength (MPa)	Young's modulus (MPa)	Elongation at break (%)
PHB/P3HB4HB (100/0)	15.2	1317.4	1.8
PHB/P3HB4HB (90/10)	9.8	1021.9	2.0
PHB/P3HB4HB (80/20)	7.8	999.5	2.5
PHB/P3HB4HB (70/30)	6.5	413.2	7.9
PHB/P3HB4HB (60/40)	3.9	211.3	18.5
PHB/P3HB4HB (50/50)	2.8	112.8	27.5
PHB/P3HB4HB (60/40)	1.2	32.9	34.2
PHB/P3HB4HB (0/100)	N/A	N/A	N/A

2.9 The effect of rice straw on properties of polymer blends

Pongputthipat et al. (2022) [15] investigated PLA/natural rubber (NR)/rice straw (RS) composites produced by casting films, as shown in Figure 2.15, all of the films have a brown color. The surface of films containing the amounts of RS (3 and 5 wt%) was smooth, whereas the amount of RS (7 wt%) had surface roughness and was porous. The morphological properties of polymer composites are shown in Figure

2.16. The surface of (a) pure PLA film had a smooth and brittle fracture. The PLA/NR blend films were demonstrated to be immiscible with NR dispersed throughout the PLA matrix. The PLA/NR/RS composite films showed RS drawn out from the polymer matrix, implying weak interfacial attachment between RS and the polymer matrix.

The mechanical properties of polymer composites are shown in Figure 2.17. The stress-strain curves exhibited ductile behavior with increasing amounts of RS (3 and 5 wt%), whereas the amount of RS (10 wt%) returned to brittle behavior, trending was equal in both directions. Compared to PLA and PLA/NR blends, Young's modulus of polymer composites increased with increasing amounts of RS (3 and 5 wt%). In comparison to PLA and PLA/NR blends, the tensile strength decreased with increasing amounts of RS compared to pure PLA and PLA/NR blends, demonstrating a weak interfacial attachment as predicted by earlier morphological properties results. In the machine direction, the elongation at break decreased with increasing amounts of RS relative to PLA/NR blends but remained greater than pure PLA [15].

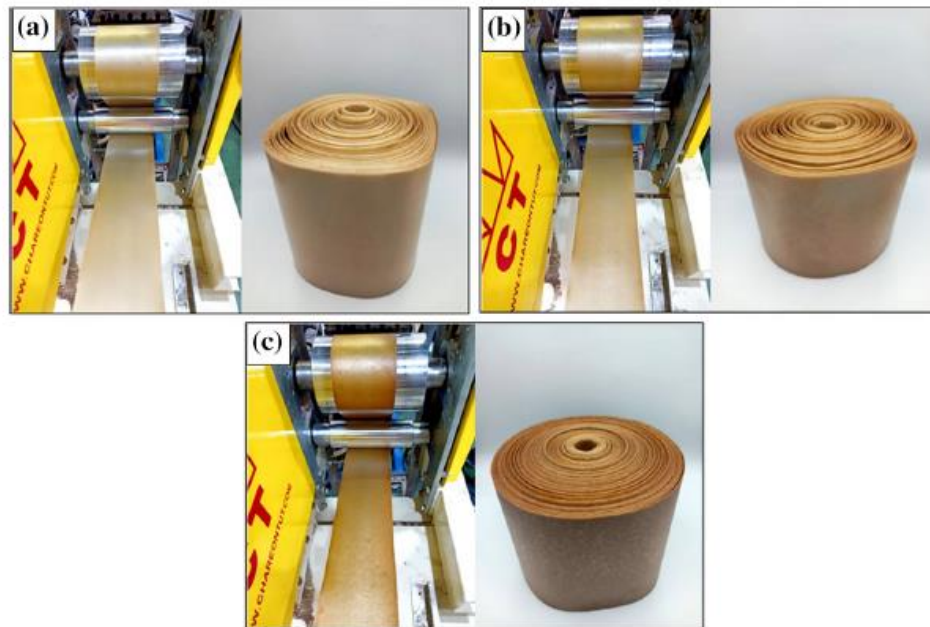


Figure 2.15 Physical properties of polymer composite films with RS content from (a) 3, (b) 5, and (c) 10 wt%, respectively [15].

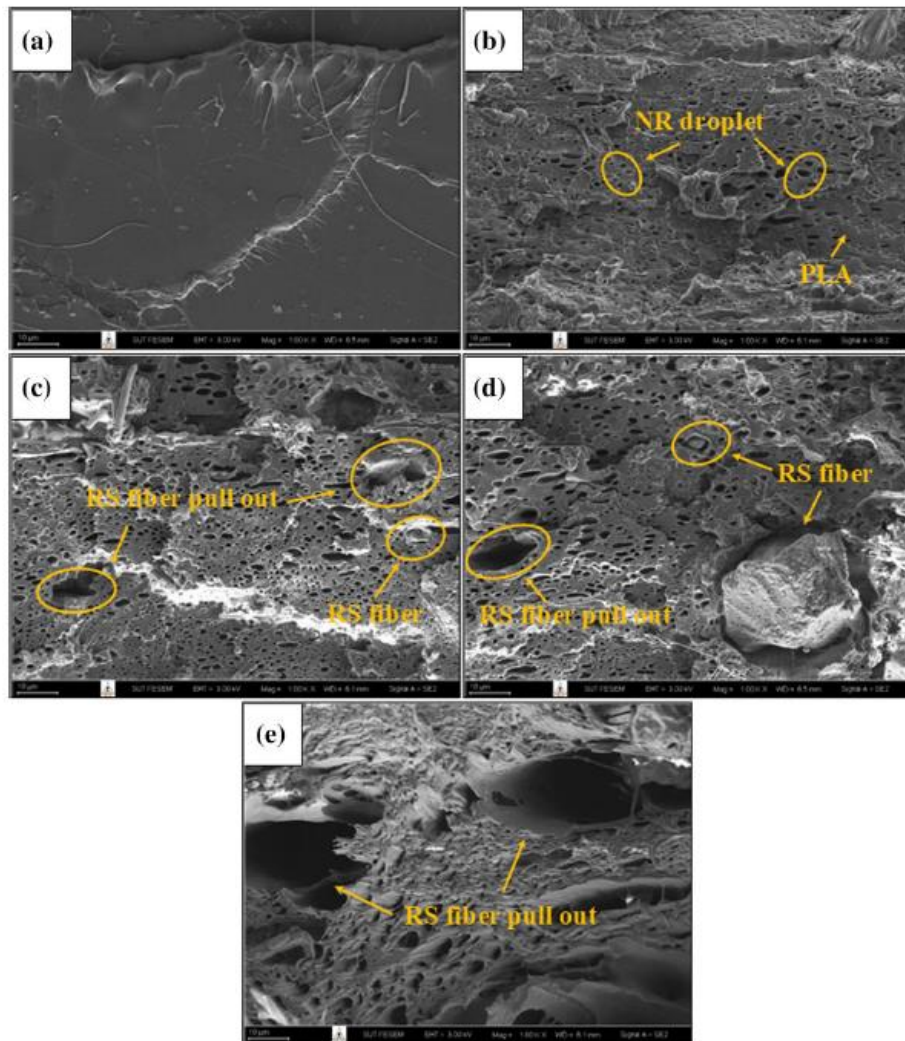


Figure 2.16 Morphological properties of (a) pure PLA and (b) PLA/NR (70/30 wt%) with increasing RS content from (c) 3, (d) 5, and (e) 10 wt%, respectively [15].

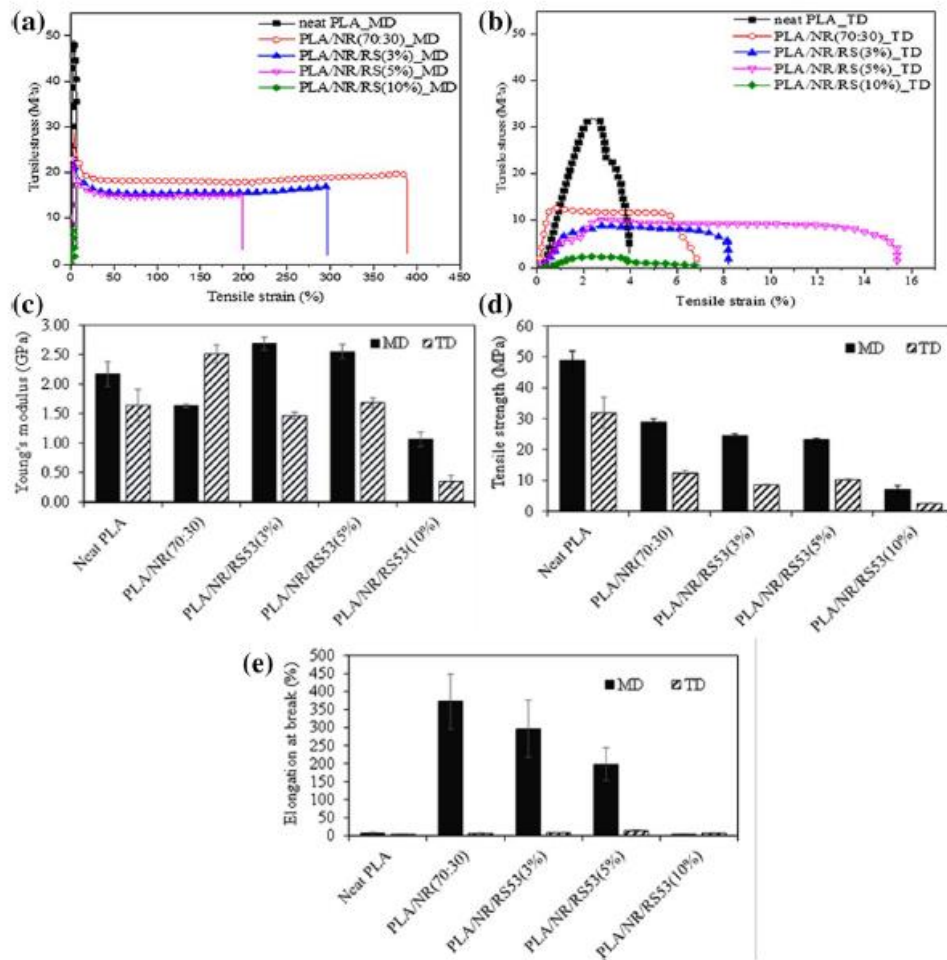


Figure 2.17 Mechanical properties of pure PLA and PLA/NR (70/30 wt%) with increasing RS content from 3, 5, and 10 wt%, stress-strain curves (a) machine direction, (b) transverse direction, (c) Young's modulus, (d) tensile strength, and (e) elongation at break [15].

Lendvai (2023) [16] investigated PLA/rapeseed straw (RSS) composites, where RSS primarily consists of lignocellulosic biomass (cellulose, hemicellulose, and lignin) similar to rice straw. PLA/RSS composites are generated by injection molding and vary the content and the size of RSS. The thermal properties of polymer composites are shown in Figure 2.18 and Table 2.7. The glass transition temperature (T_g) of polymer composites decreased with increasing the amount of RSS, indicating decreased interfacial attachment of polymer composites. The cold crystallization temperature (T_{cc}) decreased, indicating increased PLA molecular chain movement

and rearrangement into a crystal, which as RSS acted as a nucleating agent. The melting temperature (T_m) exhibited double melting peaks and was not significantly changed in both T_m , which demonstrated that melt-recrystallization occurred. The melt-recrystallization-capable instability crystal transforms into a stable crystal, which has a higher T_m with the addition of RSS. The percentage of crystallinity (X_c) increased, confirming that RSS acted as a nucleating agent and accelerated the crystallization rate. The sizes of RSS affect the percentage of crystallinity, and smaller sizes have a higher percentage of crystallinity, indicating a larger number of nucleating sites.

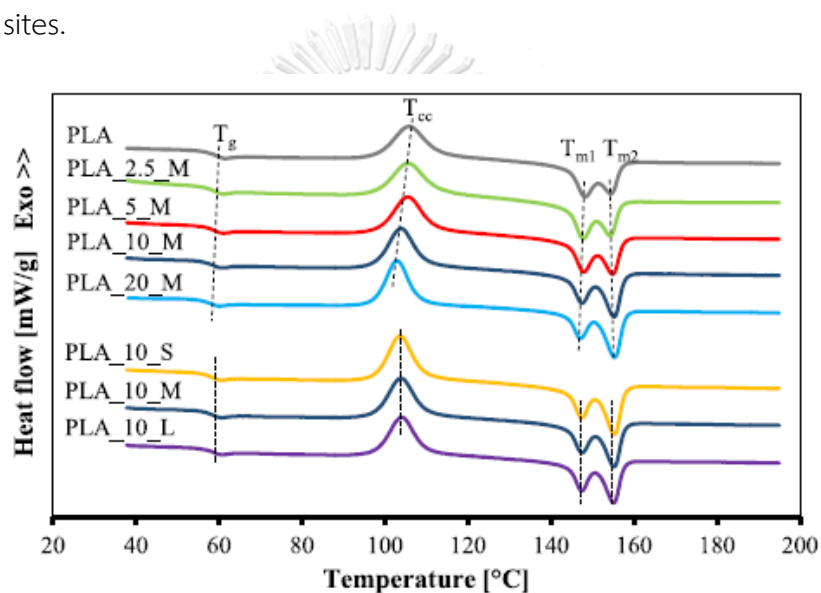


Figure 2.18 DSC thermograms of polymer composites [16].

CHULALONGKORN UNIVERSITY

Table 2.7 Thermal properties of polymer composites [16].

Polymer	T_g PLA (°C)	T_{cc} PLA (°C)	T_{m1} PLA (°C)	T_{m2} PLA (°C)	X_c PLA (%)
PLA	60.2	105.7	148.3	154.4	26.5
PLA/2.5/M	59.1	105.5	147.8	154.4	28.7
PLA/5.0/M	58.8	105.4	147.8	154.7	29.4
PLA/10.0/M	58.5	103.7	147.4	155.2	31.6
PLA/20.0/M	58.3	102.9	147.3	155.3	34.6
PLA/10.0/S	58.7	103.7	147.3	155.3	33.4
PLA/10.0/L	58.7	103.9	147.4	155.2	29.4

The morphological properties of polymer composites are shown in Figure 2.19, the pure PLA was smooth and porous. The polymer composites with increasing amounts of RSS had surface roughness, porous, and micro-fragile, indicating inadequate adhesive attachment between RSS and PLA matrix [16].

The mechanical properties of polymer composites are shown in Table 2.8. The tensile strength decreased with increasing amounts of RSS, demonstrating a weak interfacial adhesion as predicted by morphological properties, however, due to stress transfer, larger sizes demonstrated greater tensile strength than smaller and medium sizes. Young's modulus increased with increasing amounts of RSS, indicating that RSS acted as a rigid reinforcement in the PLA matrix. The elongation at break decreased as amounts of RSS increased, whereas rigid RSS obstructed PLA molecular chain movement [16].

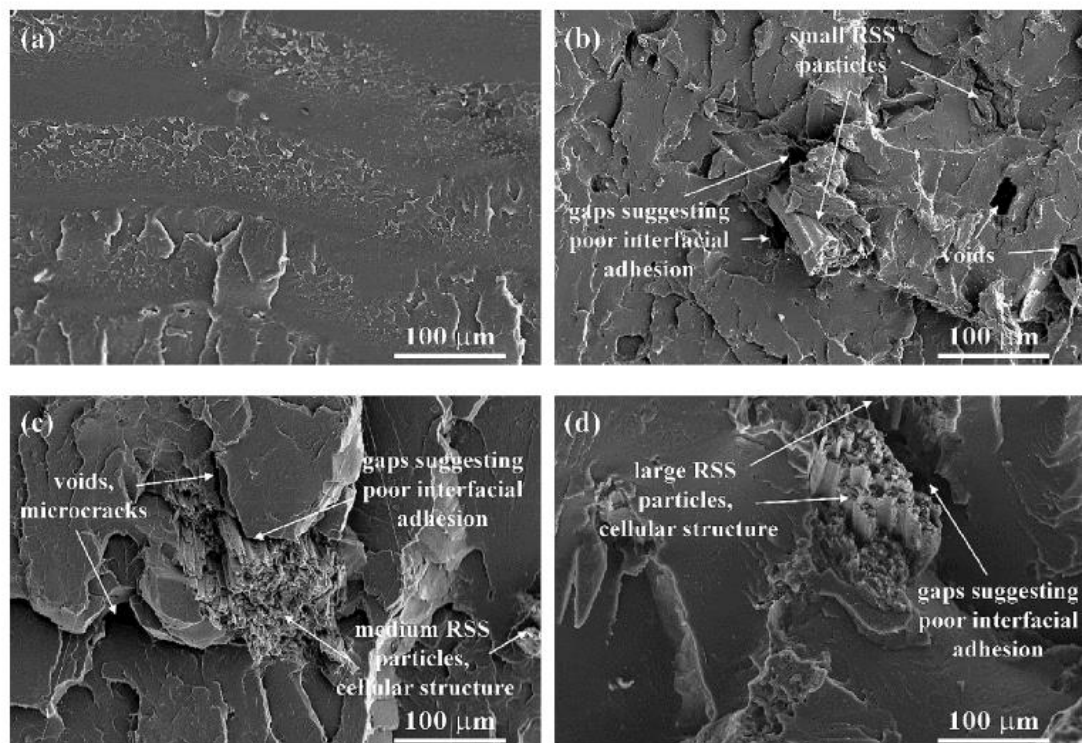


Figure 2.19 Cross-sectional SEM images of (a) pure PLA with fixed amounts of RSS (10 wt%) and vary the size of RSS (b) PLA/10.0/S, (c) PLA/10.0/M, and (d) PLA/10.0/L [16].

Table 2.8 Mechanical properties of polymer composites [16].

Polymer	Tensile strength (MPa)	Young's modulus (GPa)	Elongation at break (%)
PLA	57.3 ± 0.7	2.58 ± 0.03	4.75 ± 0.86
PLA/2.5/M	52.4 ± 0.7	2.63 ± 0.03	3.58 ± 0.47
PLA/5.0/M	50.9 ± 0.6	2.76 ± 0.06	3.08 ± 0.31
PLA/10.0/M	48.3 ± 1.4	2.99 ± 0.10	2.35 ± 0.15
PLA/20.0/M	46.5 ± 0.2	3.42 ± 0.03	1.88 ± 0.05
PLA/10.0/S	47.5 ± 0.2	3.01 ± 0.059	2.25 ± 0.29
PLA/10.0/L	49.7 ± 0.4	3.17 ± 0.04	2.12 ± 0.09

Yang et al. (2023) [11] investigated PLA/rice straw (RS) composite films produced by compression molding, RS modified with sodium hydroxide (NaOH), silane coupling agent (KBM-403), and tetraethyl orthosilicate (TEOS) treatment. In each of the three treatments, impurities such as wax, hemicellulose, and lignin were eliminated, the chemical structure was broken down into smaller fibers, and the surface roughness was roughened, which enhanced the compatibility of composites. The morphological properties are shown in Figure 2.20, (a) unmodified PLA/RS composites had a significant amount of porosity between RS and polymer matrix. After each of the three treatments, amounts of porous decreased, indicating that rough RS was embedded into the polymer matrix and that interfacial attachment in polymer composites was enhanced. TEOS treatment dispersed silica (SO₂) throughout the matrix.

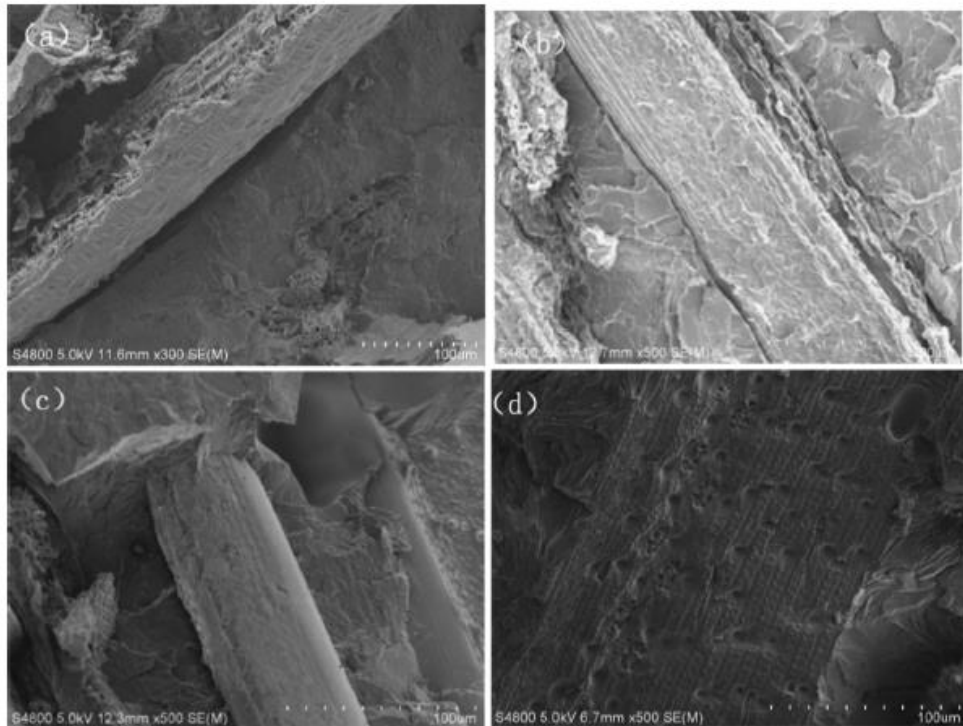


Figure 2.20 SEM images of PLA/RS composite films (a) unmodified, (b) NaOH, (c) KBM403, and (d) TEOS treatments [11].

The thermal properties of polymer composites are shown in Figure 2.21 and Table 2.9. The glass transition temperature (T_g) of polymer composites slightly increased, indicating that the transition from the amorphous phase to the crystalline phase demanded greater amounts of energy to melt. The percentage of crystallinity (X_c) increased between unmodified and each of the three treatments. The cold crystallization temperature (T_{cc}) was decreased with each of the three treatments, indicating the energy to form a crystal was decreased. During the crystallization procedure, PLA molecular chain movements were easier to arrange and form into the crystal, and the percentage of crystallinity increased.

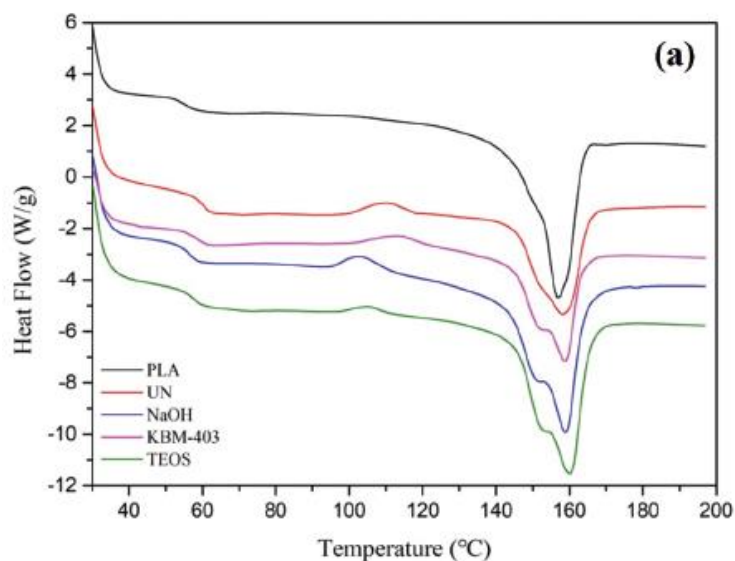


Figure 2.21 DSC thermograms of unmodified PLA and each of the three treatments [11].

Table 2.9 Thermal properties of unmodified PLA and each of the three treatments [11].

	T_g PLA (°C)	T_{cc} PLA (°C)	X_c PLA (%)
PLA	58.34	N/A	47.4
Unmodified PLA	62.03	110.28	28.0
NaOH	58.65	103.52	41.2
KBM-403	61.46	113.65	36.9
TEOS	59.85	105.37	40.6

From the literature reviews, it shows that the incorporation of flexible P3HB4HB serves to mitigate the brittleness inherent in PLA, thereby promoting a more ductile fracture behavior in the blend. Additionally, P3HB4HB functions as a nucleating agent, expediting crystallization within the PLA matrix and augmenting the overall crystallinity percentages in the polymer blend. This elevation in crystallinity percentages has the potential to improve various properties, including gas barrier properties, tensile strength, and Young's modulus. Moreover, the introduction of rice

straw fiber contributes to the enhancement of tensile strength and Young's modulus, while preserving the ductile characteristics of PLA/NR blends. Lastly, the alkaline treatment plays a crucial role in modifying the chemical structure of RS fiber by removal of lignin and hemicellulose compositions, leading to an improved interfacial adhesion between the RS fiber and polymer matrix. Additionally, it results in an increase in crystallinity percentages, further contributing to the overall enhancement of the material properties.



Chapter 3

Experiments

3.1 Materials

PLA 4043D was purchased from Ingeo™, NatureWork LLC in the USA. P3HB4HB EM10080 (density 1.26, melt flow rate (MFR) of 2.5 g/10, melting point approximately 150 °C) was purchased from Shenzhen Ecomann Biotechnology Co., Ltd. Rice straw (RS) was purchased from Thailand.

3.2 Preparation of rice straw fiber (RS)

Untreated rice straw and treated rice straw fiber were cleaned approximately five times with water to eliminate the impurities before being dried in an oven at 80 °C for 12 hours. After that, the treated rice straw fiber was prepared with an 8% sodium hydroxide solution (NaOH), added to the solution, and soaked for 12 hours. It was cleaned repeatedly to neutral (pH = 7) and dried in an oven at 80 °C for 12 h. It was ground and milled with a grinder and sieved with a mesh of 106 microns in a sieve shaker. Before mixing, untreated rice straw and treated rice straw fiber were dried in an oven.

3.3 Characterization of rice straw fiber (RS)

3.3.1 The chemical structures

The chemical structures of untreated and treated rice straw fiber were observed by a Fourier Transform Infrared Spectroscopy (FT-IR) spectrometer (PerkinElmer Spectrum GX). The samples were tested under ATR mode in the scanning wave ranging from 400 to 4000 cm^{-1} , at a resolution of 4 cm^{-1} , and with 64 scans.

3.3.2 The morphological properties

The morphologies of untreated and treated rice straw fiber were observed by field emission scanning electron microscope (FE-SEM) (FEI, Quanta™ 250 FEG-SEM,

Czech Republic). The samples were prepared on carbon tape and sputter coated with gold operating at 10 kV.

3.3.3 The thermal stability

The thermal stability of untreated and treated rice straw fiber was analyzed by a thermogravimetric analyzer (TGA) (TGA 1, Mettler-Toledo, Thailand). The sample weights used were approximately 6 to 8 mg. The samples were tested under the following conditions: a temperature scan from 25 to 800 °C and a heating rate of 10 °C/min. In all measurements, nitrogen gas was used at a flow rate of 50 mL/min.

3.4 Preparation of PLA/P3HB4HB blend films and PLA/P3HB4HB/RS composite films

The PLA and P3HB4HB were dried in an oven at 80 °C for 24 h to completely remove the moisture. The weight ratio of PLA/P3HB4HB blends was prepared following in Table 3.1.

Table 3.1 Composition of PLA/P3HB4HB blends

Polymer	Content of PLA (wt%)	Content of P3HB4HB (wt%)
PLA/P3HB4HB (100/0)	100	0
PLA/P3HB4HB (90/10)	90	10
PLA/P3HB4HB (80/20)	80	20
PLA/P3HB4HB (70/30)	70	30
PLA/P3HB4HB (60/40)	60	40
PLA/P3HB4HB (0/100)	0	100

After mixing different weight ratios, the best condition of PLA/P3HB4HB blends was chosen to mix with untreated rice straw fiber, as shown in Table 3.2. The best condition of composites was selected for comparison with the treated rice straw

fiber. The PLA, P3HB4HB, and RS were dried in an oven at 80 °C for 24 hours to completely remove the moisture.

Table 3.2 Composition of PLA/P3HB4HB/RS composites

Polymer	Content of PLA (wt%)	Content of P3HB4HB (wt%)	Content of RS (phr)
PLA/P3HB4HB/RS (the best condition/3)	The best condition		3
PLA/P3HB4HB/RS (the best condition/5)			5
PLA/P3HB4HB/RS (the best condition/7)			7

The melt blending for PLA/P3HB4HB blends and PLA/P3HB4HB/RS composites was prepared by an internal mixer. The screw speed was 50 to 70 rpm at 190 °C for 10 minutes and cut into the pellet. After that, films were created from polymer pellets previously processed using a compression molding machine (model LP20-B from Labtech Engineering Co., Ltd. (Bangkok, Thailand)). Setting the conditions following (i) pre-heat at 190 °C for 25 minutes, (ii) fully-pressed at mold temperature 190 °C and mold pressure 150 MPa for 5 minutes, and (iii) cool with water to room temperature for 30 minutes. After that, the thickness of the PLA/P3HB4HB blend and PLA/P3HB4HB/RS composite films was 190 to 200 μm .

3.5 Characterization of PLA/P3HB4HB blend and PLA/P3HB4HB/RS composite films

3.5.1 The morphological properties

The cross-sectional morphologies of pure PLA, pure P3HB4HB, PLA/P3HB4HB blend, and PLA/P3HB4HB/RS composite films were observed by field emission scanning electron microscope (FE-SEM) (FEI, QuantaTM 250 FEG-SEM, Czech Republic). The samples were cryo-fractured in liquid nitrogen onto carbon tape and sputter coated with gold operating at 10 kV.

The crystalline formation of the best condition of PLA/P3HB4HB blend, and PLA/P3HB4HB/RS composite films were observed by a polarizing optical microscope

(POM) (DMRXP, LEICA). The samples were heated from 25 to 200 °C and maintained the temperature for 5 min to eliminate the heat history. After that, the samples were rapidly cooled to the crystallization temperature at a cooling rate of 60 °C/min and then held isothermally.

3.5.2 The thermal properties

The non-isothermal properties of pure PLA, pure P3HB4HB, PLA/P3HB4HB blend, and PLA/P3HB4HB/RS composite films were observed by a differential scanning calorimeter (DSC) (Model DSC1 module, Mettler-Toledo, Switzerland). The sample weights used were approximately 6 to 8 mg. The samples were tested under the following conditions: temperature scan from -60 to 200 °C, heated to 200 °C with a heating rate of 10 °C/min, holding at 200 °C for 2 min, and cooled to -60 °C with a cooling rate of 10 °C/min (run 2 steps for eliminating the heat history). In all measurements, nitrogen gas was used at a flow rate of 50 mL/min.

3.5.3 The gas barrier properties

The oxygen transmission rate (OTR) of pure PLA, pure P3HB4HB, PLA/P3HB4HB blend, and PLA/P3HB4HB/RS composite films were obtained by an oxygen permeation analyzer (OX-TRAN 2/21, Mocon, USA) following ASTM D3985. The samples were tested at 23 °C, 0% relative humidity (RH), using an oxygen flow rate of 40 cm³/min. The samples were cut into a circle mold of equipment with a 5 cm² surface area and the thickness was 195 ± 5 μm which the films were measured 5 positions and repeated 5 times.

The water vapor transmission rate (WVTR) of pure PLA, pure P3HB4HB, PLA/P3HB4HB blend, and PLA/P3HB4HB/RS composite films were obtained by a water vapor permeation analyzer (PERMATRAN-W Model 398, Mocon, USA) following ASTM E398. The samples were tested at 37.8 °C, 90% relative humidity (RH). The samples were cut into a circle mold of equipment with a 5 cm² surface area and the thickness was 195 ± 5 μm which the films were measured 5 positions and repeated 5 times.

3.5.4 The mechanical properties

The tensile properties of pure PLA, pure P3HB4HB, PLA/P3HB4HB blend, and PLA/P3HB4HB/RS composite films were obtained by a Universal testing machine (UTM) (Instron 5567, NY, USA) following ASTM D882. The samples were tested with a 1kN load cell, a gauge length of 50 mm, and the grip separation rates are 50 mm/min. The samples were cut into rectangular shapes with a 20 mm width, a 100 mm length, and $195 \pm 5 \mu\text{m}$ thickness which the films were measured 5 positions and repeated 5 times.



Chapter 4

Results and Discussion

4.1 Characterization of rice straw fiber (RS)

4.1.1 The chemical structures

The chemical structures of untreated and treated rice straw fiber were investigated by Fourier transform infrared spectroscopy (FT-IR). In Figure 4.1, A broad band peak at 3358 cm^{-1} attributed to a hydroxyl group (-OH absorption) of both untreated and treated rice straw. Notably, there was a remarkably increase in the peak intensity of treated rice straw because some hemicellulose and lignin were eliminated during alkali treatment leading to the more pronounced observation of this peak. The peak at 1732 cm^{-1} , attributed to carboxyl or acetyl groups (C=O stretching) in hemicellulose and lignin, exhibited a significant decrease [11]. Acetyl groups play a crucial role in connecting lignin and hemicellulose, serving as a primary barrier to the hydrolysis of hemicellulosic polysaccharides [17]. The decrease in the intensity of the acetyl groups' peak provides evidence that NaOH treatment enhanced accessibility to cellulose. The carbonyl groups (C=O stretching) of aromatic ketones in lignin (amorphous lignin) were identified at 1646 and 1610 cm^{-1} , demonstrating a notable decrease and indicating a reduction in the proportion of amorphous lignin [18].

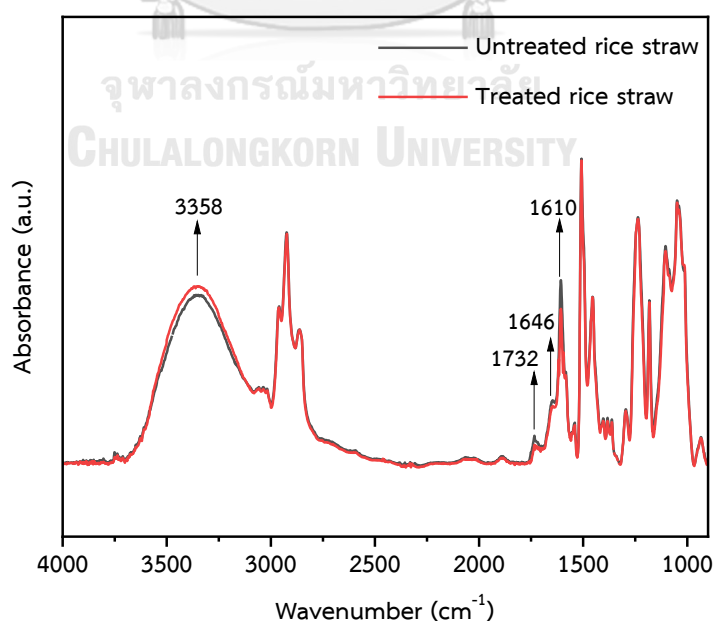


Figure 4.1 FT-IR spectra of untreated and treated rice straw fiber.

4.1.2 The morphological properties

The morphologies of untreated and treated rice straw fiber were investigated by field emission scanning electron microscopy (FE-SEM) at 150x magnification, as depicted in Figure 4.2. (a) Untreated rice straw exhibited apparently short fibers with a diameter distribution ranging from 50 to 95 μm . Conversely, following treatment with NaOH solution, (b) the treated rice straw displayed a reduced diameter within the range of 35 to 80 μm and exhibited the formation of small branches. This structural transformation is anticipated to augment the surface area interactions between fibers and polymer matrices.

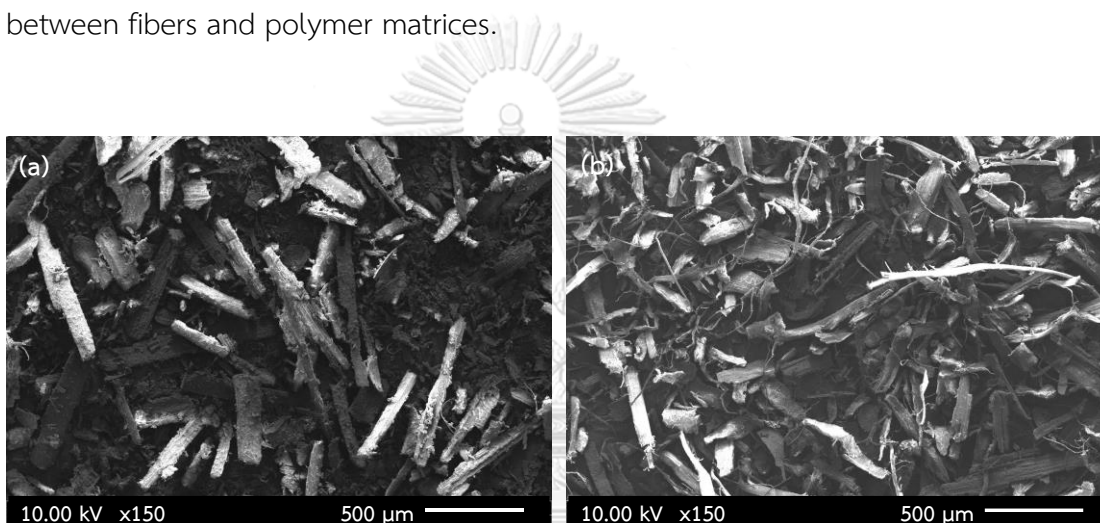


Figure 4.2 FE-SEM images of (a) untreated and (b) treated rice straw fiber at 150 magnification.

4.1.3 The thermal stability

The thermal stability of both untreated and treated rice straw fiber was investigated by thermogravimetric analysis (TGA). TGA and DTG curves, depicted in Figure 4.3, illustrate distinct thermal degradation characteristics. In the case of untreated rice straw fiber, multiple degradation steps were observed, contrasting with the treated rice straw. The analysis revealed the presence of bound moisture and volatile species in the temperature range of 35-160 $^{\circ}\text{C}$ for both untreated and treated rice straw [19]. The treated rice straw exhibited a reduction in bound moisture on its surface and a decrease in volatile species content, attributed to the removal of certain volatiles during alkaline treatment. Furthermore, major degradation occurred

in a temperature range of 180 to 230 °C, primarily due to the thermal decomposition of hemicellulose and cleavage of glycoside linkages in cellulose [20, 21]. Lignin, characterized by higher thermal stability compared to hemicellulose and cellulose, displayed decomposition at higher temperatures, marked by two dominant peaks at 290 and 348 °C, extending up to 530 °C in the DTG curve [20, 22]. Regarding the area under the DTG curve, it represents the concentration of materials inside the sample. When compared the area under the DTG curve in a temperature range of approximately 290-400 °C between untreated and treated RS fiber, primarily involving lignin decomposition, a higher area was observed for the treated RS fiber. This phenomenon is ascribed to the dilution in the lignin concentration of untreated RS fiber, leading to reduced intensity and area under the peak in this specific temperature range. Moreover, the thermal stability of the treated rice straw was notably higher, with a T_{d10} value of 291 °C, compared to the untreated rice straw, which exhibited a T_{d10} value of 221 °C.

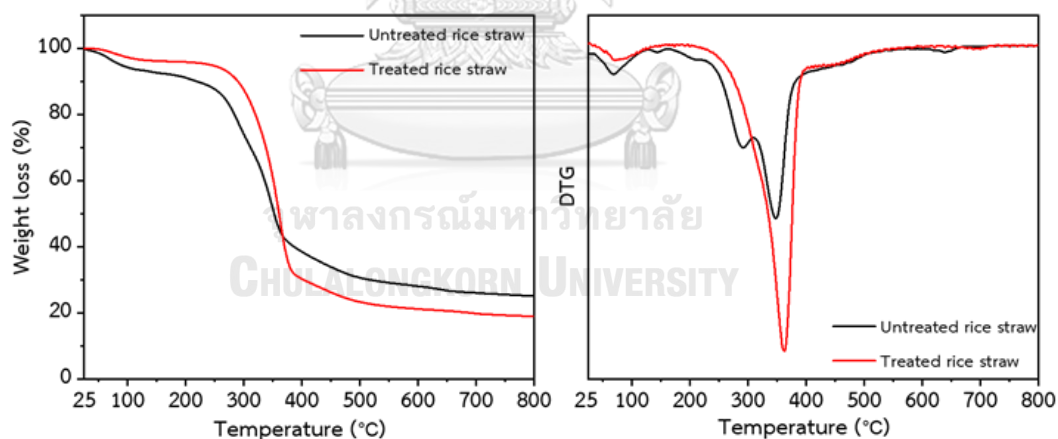


Figure 4.3 TGA and DTG curves of untreated and treated rice straw fiber.

4.2 Characterization of PLA/P3HB4HB blend films

4.2.1 The morphological properties

The cross-sectional morphologies of PLA/P3HB4HB blend films were investigated by field emission scanning electron microscopy (FE-SEM) at 3000x magnification. In Figure 4.4, cross-sectional FE-SEM images reveal the following: (a)

Pure PLA displayed homogeneous textures and smooth surfaces. (b) PLA/P3HB4HB blends (90/10) exhibited a rough surface with small P3HB4HB domains dispersed in the matrix, showcasing initial ductile fractures. (c-e) With an increase in P3HB4HB content from 20 to 40 wt%, the roughness significantly escalated, accompanied by an augmentation in the size of P3HB4HB domains. These heterogeneous phases indicated immiscible behavior between PLA and P3HB4HB. Additionally, the presence of vacancies in PLA/P3HB4HB blends was observed, attributed to the cracking process and weak interfacial adhesion between PLA and P3HB4HB, evidenced by the surrounding gap between the P3HB4HB domain and PLA phase [23, 24]. (f) Pure P3HB4HB displayed a rougher surface compared to pure PLA, featuring small spherical particles dispersed in the matrix.

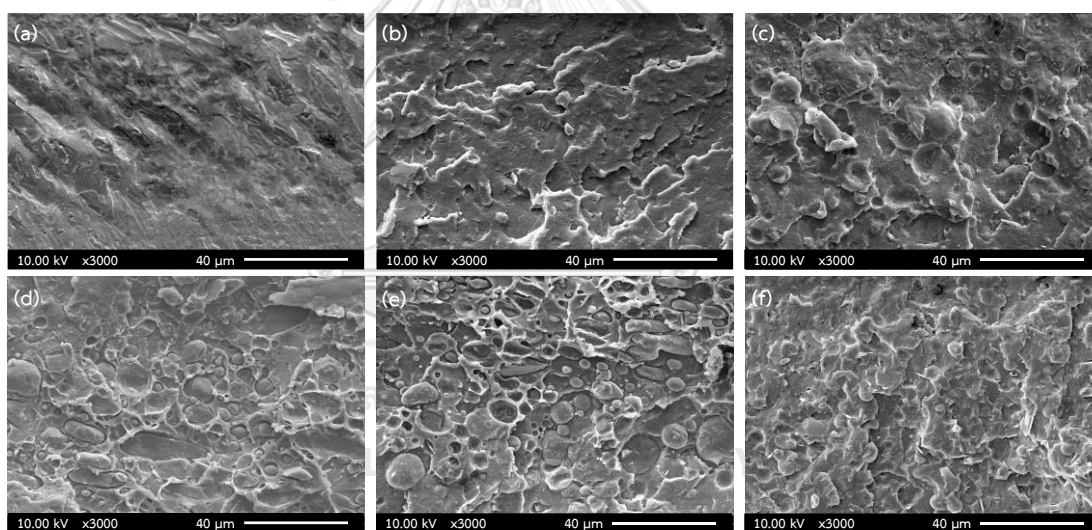


Figure 4.4 Cross-sectional FE-SEM images of (a) pure PLA, PLA/P3HB4HB blends: (b) 90/10, (c) 80/20, (d) 70/30, (e) 60/40, and (f) pure P3HB4HB at 3000 magnification.

4.2.2 The thermal properties

The thermal properties of PLA/P3HB4HB blend films were investigated by differential scanning calorimetry (DSC). Figure 4.5 illustrates DSC thermograms of PLA/P3HB4HB blends, and the corresponding glass transition temperatures (T_g), melting temperatures (T_m), cold crystallization temperatures (T_{cc}), and crystallinity percentages (X_c) are presented in Table 4.1, The T_g values of pure PLA and pure P3HB4HB were

observed at 60 and -33 °C, respectively. With an increasing P3HB4HB content in the blends, there was a trend of decreasing T_g for PLA to 58, 57, 57, and 56 °C for 90/10, 80/20, 70/30, and 60/40 PLA/P3HB4HB, respectively. This reduction can be attributed to the incorporation of the more flexible structures of P3HB4HB into the PLA matrix [3]. However, the T_g of P3HB4HB in PLA/P3HB4HB blends at 70/30 and 60/40 remained unchanged, indicating an immiscible blend between PLA and P3HB4HB [14]. Additionally, the T_g of P3HB4HB was not observed in PLA/P3HB4HB blends at 90/10 and 80/20. The T_{cc} of pure PLA was 117 °C and exhibited a decreasing trend with increasing P3HB4HB content, suggesting a high crystallization rate [7]. The T_m values of pure PLA and pure P3HB4HB were 149 and 142 °C, respectively. In PLA/P3HB4HB blends at 80/20, 70/30, and 60/40, a double melting peak was observed, representing the T_m of PLA and P3HB4HB in the blend. Furthermore, the T_m of both polymers increased with the addition of P3HB4HB content, attributed to the bulky and large size of P3HB4HB hindering the flexibility of the polymer chain [25]. The crystallinity percentages (X_c) of PLA/P3HB4HB blends decreased as an increase in P3HB4HB content, as P3HB4HB domains may restrict the mobility of the polymer structure and impede reorganization into a crystalline form [23].

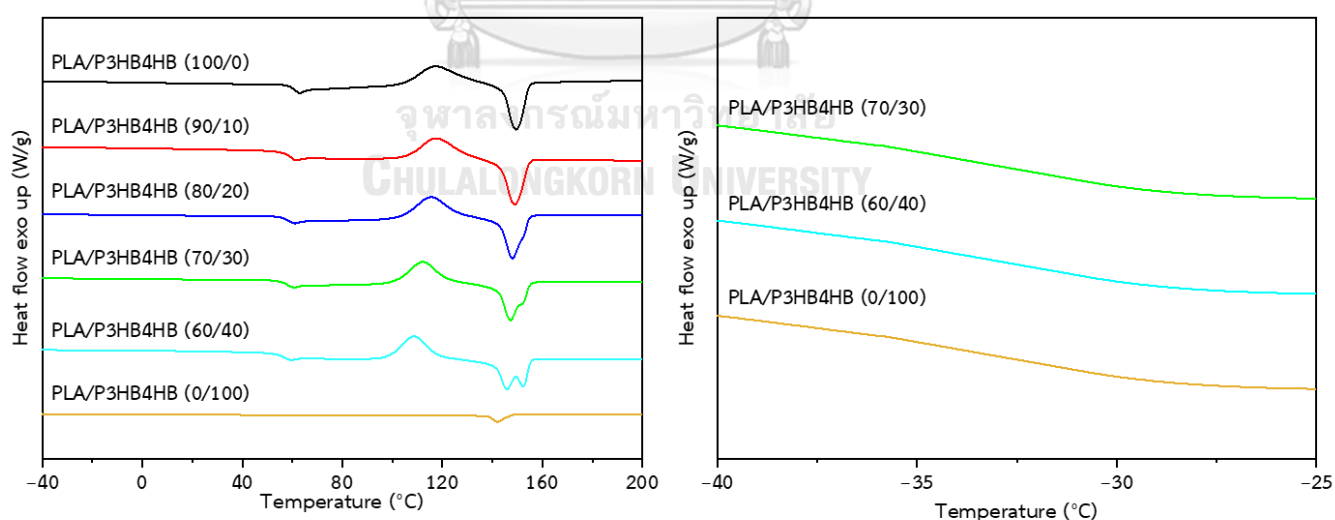


Figure 4.5 DSC thermograms of PLA/P3HB4HB blend films.

Table 4.1 Thermal properties of PLA/P3HB4HB blend films.

Polymer	T _g P3HB4HB (°C)	T _g PLA (°C)	T _{cc} PLA (°C)	T _m P3HB4HB (°C)	T _m PLA (°C)	X _c blend (%)
PLA/P3HB4HB (100/0)	N/A	60	117	N/A	149	9.4
PLA/P3HB4HB (90/10)	N/A	58	117	N/A	149	7.1
PLA/P3HB4HB (80/20)	N/A	57	115	148	152	1.7
PLA/P3HB4HB (70/30)	-33	57	112	147	152	0.1
PLA/P3HB4HB (60/40)	-33	56	109	146	152	0.1
PLA/P3HB4HB (0/100)	-33	N/A	N/A	142	N/A	0.3

4.2.3 The gas barrier properties

The oxygen transmission rate (OTR) of PLA/P3HB4HB blend films was investigated by an oxygen permeation analyzer. Figure 4.6 presents a summary of the OTR values for the blends. The OTR value for pure PLA was 77 cc/m².day and increased to 403 cc/m².day with a 40 wt% increase in P3HB4HB. This rise in OTR can be attributed to the increased presence of the lower gas barrier P3HB4HB in the blend, which itself has the highest OTR value of 534 cc/m².day [3]. These findings align with observations in the blend morphologies discussed in Section 4.2.1, where gaps between PLA matrices and P3HB4HB domains indicate weak interfacial adhesion between the two polymer phases, potentially allowing oxygen gas flow throughout the films.

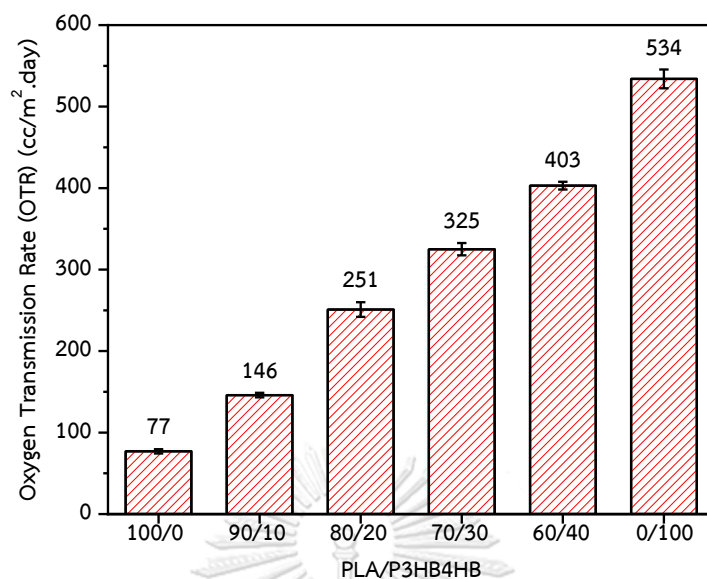


Figure 4.6 Oxygen transmission rate (OTR) of PLA/P3HB4HB blend films.

The water vapor transmission rate (WVTR) of PLA/P3HB4HB blend films was investigated using a water vapor permeation analyzer. In Figure 4.7, the WVTR value of pure PLA was $151 \text{ g/m}^2 \cdot \text{day}$ markedly increased to $318 \text{ g/m}^2 \cdot \text{day}$ with a 40 wt% increase in P3HB4HB content in the blends. This increase in the WVTR was attributed to the hydrophobic nature of P3HB4HB [3]. As evident in Section 4.2.1, higher surrounding gaps between PLA matrices and P3HB4HB domains correlated with higher WVTR values in the blends.

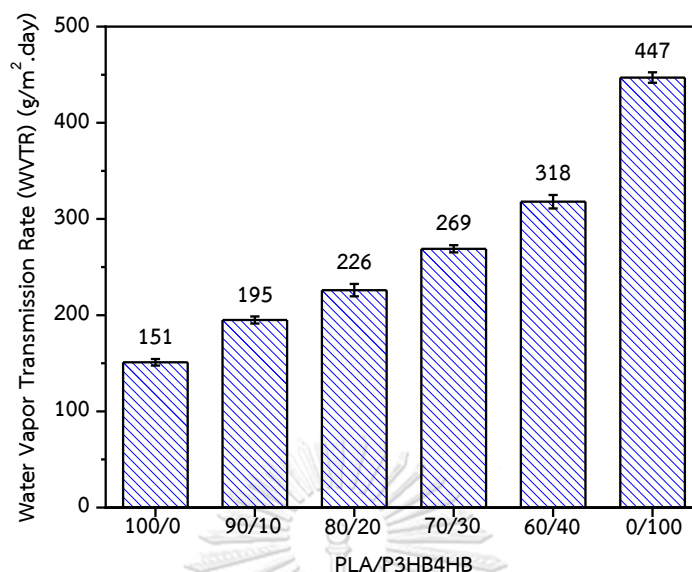


Figure 4.7 Water vapor transmission rate (WVTR) of PLA/P3HB4HB blend films.

4.2.4 The mechanical properties

The mechanical properties of PLA/P3HB4HB blend films were investigated using a universal testing machine (UTM) under a tension mode. In Figure 4.8, the stress-strain curves revealed an increase in the elongation at break for PLA/P3HB4HB blends (90/10). This enhancement was attributed to the small proportion of P3HB4HB, which did not induce significant phase separation in the blend. The flexibility of the P3HB4HB molecular chain contributed to an overall increase in the flexibility of the blends [3]. However, an excess of 10 wt% P3HB4HB resulted in noticeable phase separation (see SEM micrographs in section 4.2.1), indicating larger P3HB4HB domains. This led to weakened interfacial adhesion between PLA and P3HB4HB domains, causing poor stress transfer [23]. Consequently, there was a decrease in the tendency of elongation at break, as well as in the values of tensile strength, Young's modulus, and toughness of the blends. These trends were consistent with the addition of P3HB4HB, except in the case of the PLA/P3HB4HB 90/10 blend, which exhibited a synergistic behavior in toughness. All values are provided in Table 4.2.

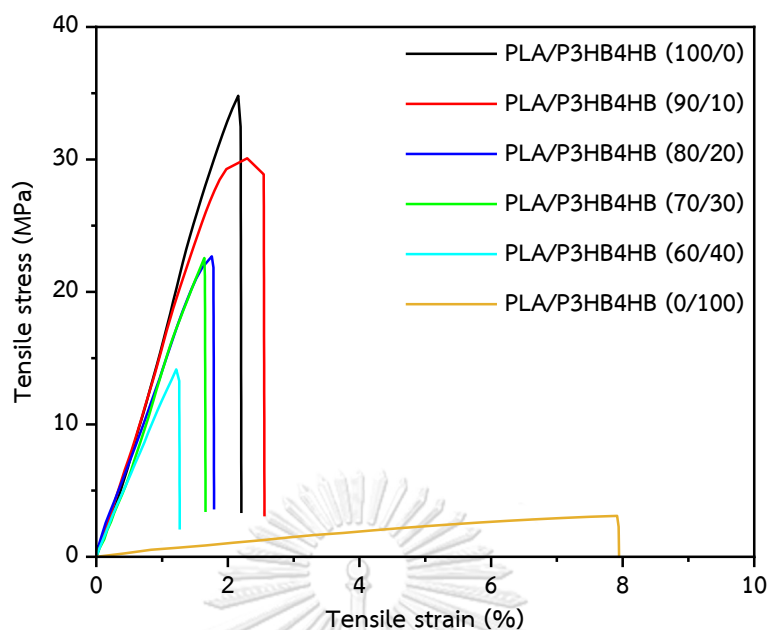


Figure 4.8 Mechanical properties of PLA/P3HB4HB blend films.

Table 4.2 Mechanical properties of PLA/P3HB4HB blend films.

Polymer	Young's modulus (GPa)	Tensile strength (MPa)	Elongation at break (%)	Toughness (J/m ³)
PLA/P3HB4HB (100/0)	1.8 ± 0.1	35.0 ± 1.1	2.2 ± 0.6	22.0 ± 0.9
PLA/P3HB4HB (90/10)	1.5 ± 0.4	30.1 ± 0.7	2.6 ± 0.4	30.6 ± 0.9
PLA/P3HB4HB (80/20)	1.4 ± 0.2	22.7 ± 0.7	1.8 ± 0.3	13.5 ± 0.8
PLA/P3HB4HB (70/30)	1.4 ± 0.1	21.8 ± 0.5	1.7 ± 0.2	9.4 ± 0.6
PLA/P3HB4HB (60/40)	1.1 ± 0.2	13.3 ± 0.3	1.3 ± 0.2	5.0 ± 0.4
PLA/P3HB4HB (0/100)	0.5 ± 0.1	7.9 ± 0.2	7.9 ± 0.5	10.3 ± 2.8

4.3 Characterization of PLA/P3HB4HB/RS composite films

4.3.1 The morphologies properties

The cross-sectional morphologies of PLA/P3HB4HB/RS composite films were investigated by field emission scanning electron microscopy (FE-SEM) at 3000x magnification. In Figure 4.9, cross-sectional FE-SEM images reveal the following: (a) PLA/P3HB4HB blend (90/10) exhibited a rough surface with small P3HB4HB domains dispersed in the matrix. (b-d) Upon the addition of untreated rice straw fiber (RS) ranging from 3 to 7 phr, gaps between RS fiber and polymer matrix were observed, indicating weak interfacial adhesion [16]. Especially, (d) PLA/P3HB4HB/RS composite (90/10/7 untreated) exhibited the formation of an agglomeration of RS. Regarding branch characteristics of treated RS fiber, (e) PLA/P3HB4HB/RS composite (90/10/3 treated) exhibited a thorough coverage of the RS fiber by the polymer matrix, suggesting an enhancement in interfacial adhesion between RS fiber and polymer matrix [11].

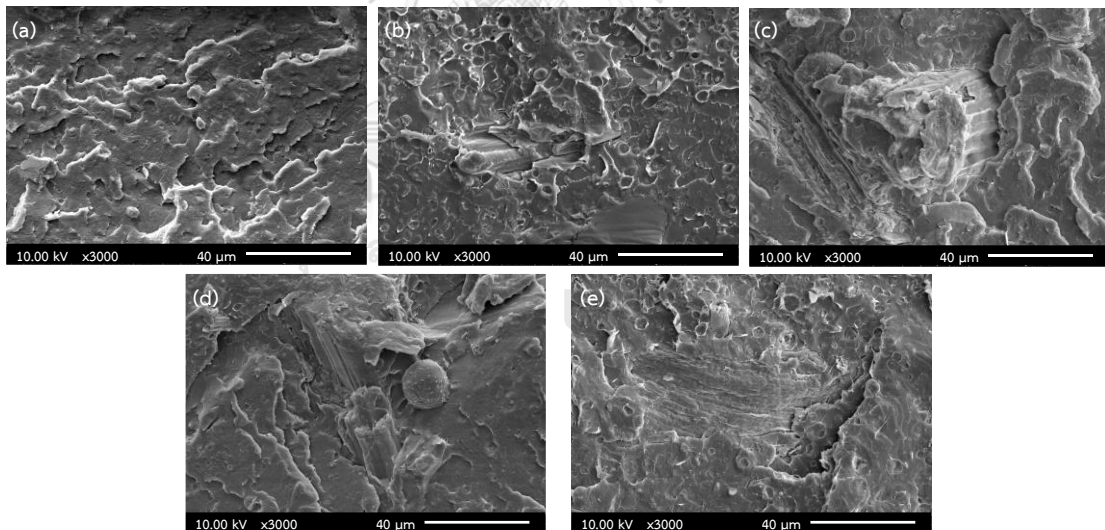


Figure 4.9 Cross-sectional FE-SEM images of (a) PLA/P3HB4HB blend, PLA/P3HB4HB/RS composites: (b) 90/10/3 untreated, (c) 90/10/5 untreated, (d) 90/10/7 untreated, and (e) 90/10/3 treated at 3000 magnification.

4.3.2 The crystalline formation in PLA/P3HB4HB blend and PLA/P3HB4HB/RS composites

Crystalline formation of PLA/P3HB4HB blend (90/10) and PLA/P3HB4HB/RS composite films were examined using a polarizing optical microscope (POM). The crystalline growth of the films was initiated at 120 °C and maintained isothermally for 5 mins, the photographs were recorded at 0, 2, and 5 min. In Figure 4.10, (a0-a2) PLA/P3HB4HB blend (90/10) exhibited luminous spots, representing crystalline forming at 2 min and increasing when reaching at 5 min. Upon the addition of untreated RS, (b0-b2 and c0-c2) PLA/P3HB4HB/RS composites at 90/10/3 and 90/10/5, displayed a decrease in crystal density, corresponding to the observed reduction in crystallinity percentages (X_c) from DSC results. Conversely, (d0-d2) PLA/P3HB4HB/RS composite (90/10/3) with treated RS showed an increase in crystal density, particularly around the branches of the rice straw fiber. This can be attributed to the removal of amorphous lignin, leading to an enhancement in the X_c of the composite filled treated RS.

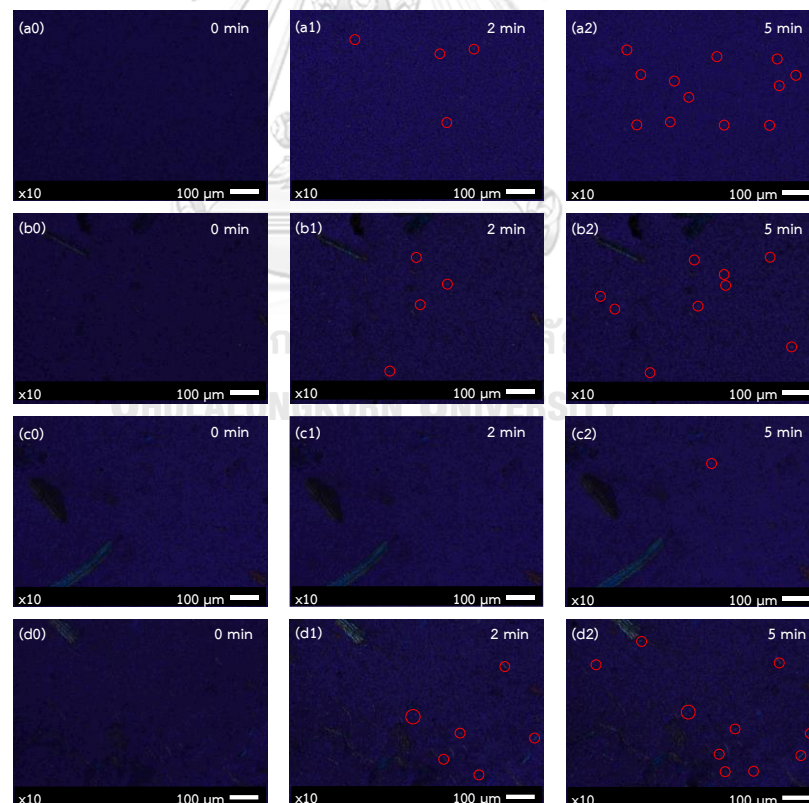


Figure 4.10 POM images of (a) PLA/P3HB4HB blend (90/10) and composites filled with untreated RS (b) 3 wt%, (c) 5 wt%, and (d) treated RS 3wt% at 120 °C, for a duration of = (a0, b0, c0, d0) 0 min, (a1, b1, c1, d1) 2 mins, and (a2, b2, c2, d2) 5 mins

4.3.3 The thermal properties

The thermal properties of PLA/P3HB4HB/RS composite films were investigated by differential scanning calorimetry (DSC). Figure 4.11 illustrates DSC thermograms of PLA/P3HB4HB/RS composites, and the corresponding T_g , T_m , T_{cc} , and X_c are presented in Table 4.3. The T_g of PLA in PLA/P3HB4HB blend (90/10) was measured at 58 °C. The introduction of untreated and treated rice straw fiber (RS) into the blends did not impact the T_g values. The T_{cc} of PLA in PLA/P3HB4HB blend (90/10) was 117 °C and increased to 119 and 120 °C with the inclusion of untreated RS (3 phr) and treated RS (3 phr), respectively, suggesting a slow crystallization rate [7]. However, the T_{cc} of PLA in PLA/P3HB4HB/RS composites at 90/10/5 and 90/10/7 untreated remained unchanged. The T_m of PLA in PLA/P3HB4HB/RS composites exhibited no significant changes, and the T_m of P3HB4HB was not observed. The X_c of PLA/P3HB4HB/RS composites decreased with the addition of untreated RS, attributed to the amorphous lignin restricting the nucleation between cellulosic species in the RS and polymer matrix during the arrangement of molecules in crystalline form [26, 27]. Furthermore, the X_c of PLA/P3HB4HB/RS composite (90/10/3 treated) increased compared to PLA/P3HB4HB/RS composite (90/10/3 untreated), suggesting the removal of an amorphous lignin leading to more efficient crystalline formation.

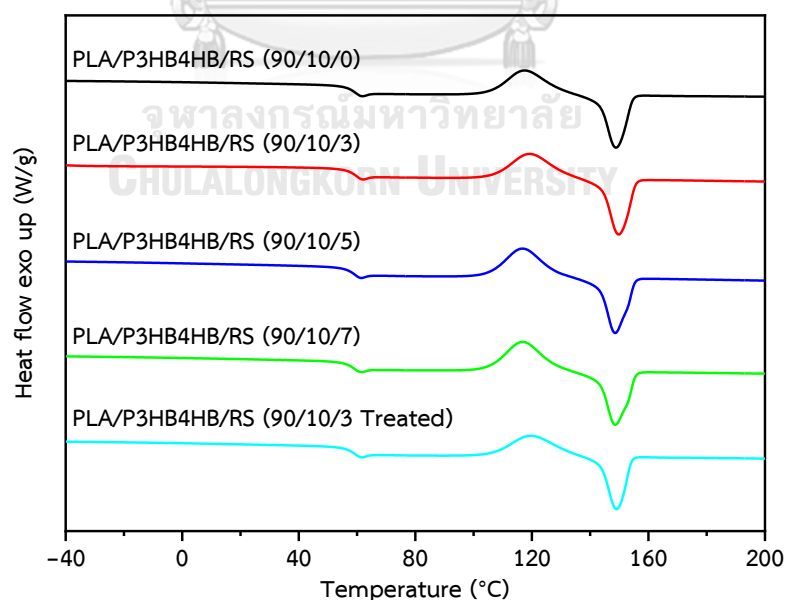


Figure 4.11 DSC thermograms of PLA/P3HB4HB blend (90/10) and PLA/P3HB4HB/RS composite films.

Table 4.3 Thermal properties of PLA/P3HB4HB blend (90/10) and PLA/P3HB4HB/RS composite films.

Polymer	T _g P3HB4HB (°C)	T _g PLA (°C)	T _{cc} PLA (°C)	T _m P3HB4HB (°C)	T _m PLA (°C)	X _c blend (%)
PLA/P3HB4HB (90/10)	N/A	58	117	N/A	149	7.1
PLA/P3HB4HB/RS (90/10/3 untreated)	N/A	58	119	N/A	149	3.0
PLA/P3HB4HB/RS (90/10/5 untreated)	N/A	58	117	N/A	148	0.6
PLA/P3HB4HB/RS (90/10/7 untreated)	N/A	58	117	N/A	148	0.7
PLA/P3HB4HB/RS (90/10/3 treated)	N/A	58	120	N/A	149	3.7

4.3.4 The gas barrier properties

Figure 4.12 provides a summary of the OTR values for the composites. The OTR value for PLA/P3HB4HB blends (90/10) was 146 cc/m².day and showed an increasing trend with the addition of untreated RS fiber. This increase in OTR can be ascribed to the presence of gaps between the RS fiber and the polymer matrix, indicating weak interfacial adhesion between the two phases and the potential for oxygen gas to flow through the films. Moreover, a pronounced increase in OTR value was notably observed with the addition of 7 phr untreated RS fiber, reaching 1333 cc/m².day. This was attributed to the formation of an agglomeration of RS fiber, as observed in the SEM composite morphologies in Section 4.3.1. In contrast, the incorporation of 3 phr treated RS fiber led to a decrease in the OTR value for PLA/P3HB4HB/RS (90/10/3 treated) compared to composites filled with 3, 5, and 7 phr untreated RS fiber. This decrease corresponds to the comprehensive coverage of the RS fiber by the polymer matrix, effectively blocking the flow of oxygen gas throughout the films.

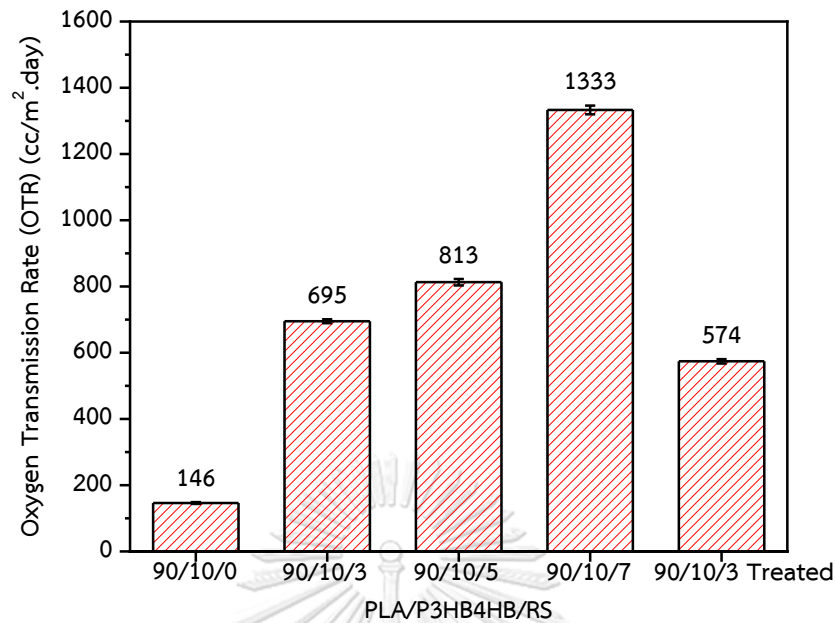


Figure 4.12 Oxygen transmission rate (OTR) of PLA/P3HB4HB blend (90/10) and PLA/P3HB4HB/RS composite films.

In Figure 4.13, the WVTR value for PLA/P3HB4HB blends (90/10) was 198 g/m².day and increased to 222 g/m².day with the addition of 3 phr untreated RS fiber. This increase was attributed to the gaps between RS fiber and the polymer matrix, allowing the easy flow of water vapor throughout the films. Furthermore, a reduction in the water vapor transmission rate (WVTR) of the composites was noted with an increase in untreated RS. This phenomenon was attributed to the dominance of hydroxyl groups in the hemicellulose and cellulose structure, enhancing water absorption. Thus, hydroxyl groups in RS act as a barrier, playing a role in impeding the flow of water vapor throughout the films [28]. Additionally, the WVTR value for PLA/P3HB4HB/RS composites could be further reduced by incorporating treated RS fiber at 3 phr, which was observed a value of 156 g/m².day. This reduction aligned with the comprehensive coverage of the RS fiber by the polymer matrix, resulting in an improved interfacial adhesion between RS fiber and polymer matrix and effectively blocking the flow of water vapor throughout the films.

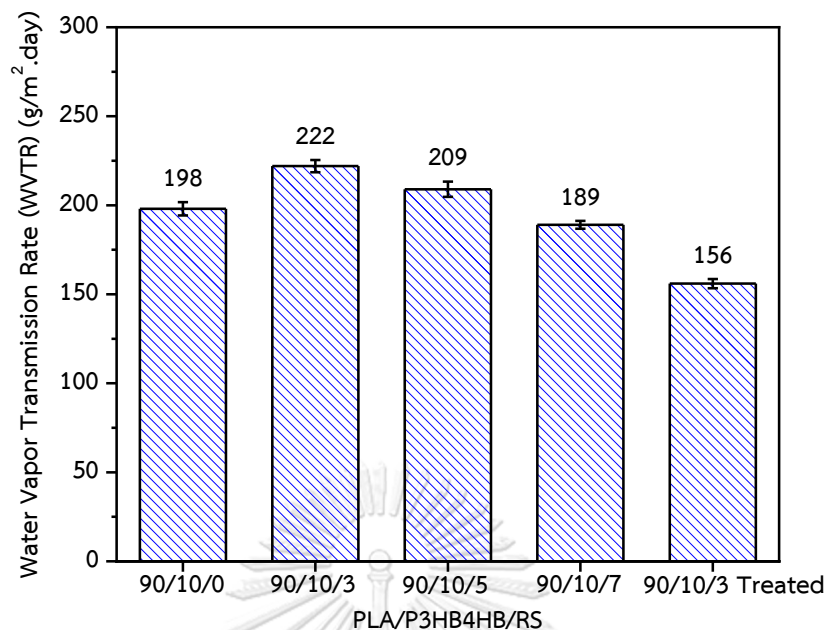


Figure 4.13 Water vapor transmission rate (WVTR) of PLA/P3HB4HB blend (90/10) and PLA/P3HB4HB/RS composite films.

4.3.5 The mechanical properties

In Figure 4.14, the stress-strain curves of PLA/P3HB4HB blend (90/10) and composites revealed an increase in young's modulus with the addition of 3, and 5 phr untreated RS fiber. This enhancement was attributed to ability to transmit and distribute the applied stress to RS fiber, thereby enhancing the stiffness of the composites [28]. Typically, a decrease in crystallinity tends to lower the modulus and strength of materials. Nevertheless, in this study, no reduction in the mechanical properties of PLA/P3HB4HB composites was observed. This is attributed to the dominating influence of the high stiffness RS fiber, outweighing the minor decrease in crystallinity from 7.1% to 0.7% in the composites. Additionally, the elongation at break of the composites decreased with an increase in untreated RS fiber, as the addition of more rigid fiber resulted in reduced flexibility of the composites. However, an increase in strain for the composites was noted upon incorporating 3 phr treated RS fiber, as the alkali treatment enhanced the flexibility of RS, facilitating greater flexibility in the composite. Furthermore, the tensile strengths of the composites remained unchanged, except when adding 7 phr untreated RS fiber, which led to a decrease in the strength of the composite due to fiber agglomeration causing poor stress transfer [29]. Finally, the toughness of the composites exhibited a decreasing trend with the inclusion of untreated RS fiber. However, in comparison to untreated RS fiber, the

addition of 3 phr treated RS fiber resulted in an increase in toughness. This was attributed to the thorough coverage of the RS fiber by the polymer matrix, facilitating greater interfacial adhesion between RS fiber and polymer matrix. All values are provided in Table 4.4.

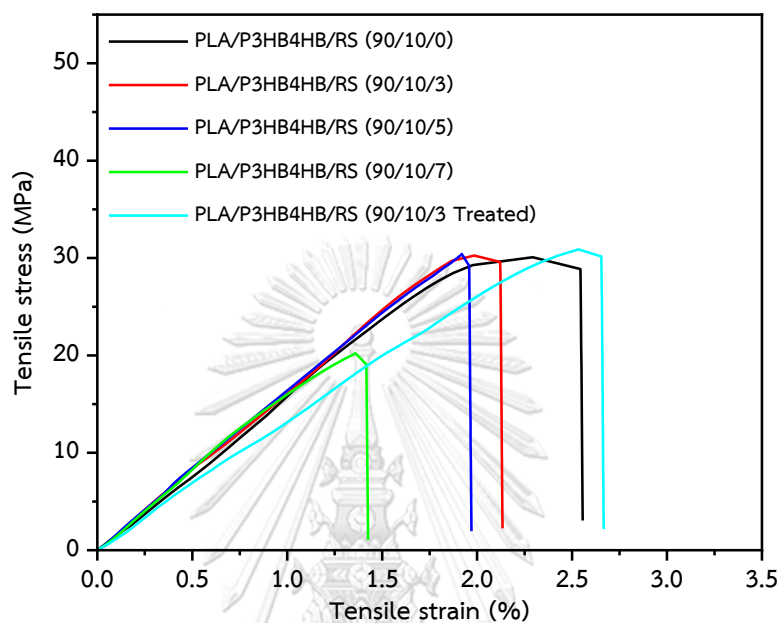


Figure 4.14 Mechanical properties of PLA/P3HB4HB blend (90/10) and PLA/P3HB4HB/RS composite films.

Table 4.4 Mechanical properties of PLA/P3HB4HB blend (90/10) and PLA/P3HB4HB/RS composite films.

Polymer	Young's modulus (GPa)	Tensile strength (MPa)	Elongation at break (%)	Toughness (J/m^3)
PLA/P3HB4HB (90/10)	1.5 ± 0.1	30.1 ± 0.7	2.6 ± 0.4	30.6 ± 0.9
PLA/P3HB4HB/RS (90/10/3 untreated)	1.7 ± 0.4	30.3 ± 1.5	2.1 ± 0.1	22.1 ± 0.8
PLA/P3HB4HB/RS (90/10/5 untreated)	1.7 ± 1.2	30.4 ± 2.7	2.0 ± 0.3	18.0 ± 0.7
PLA/P3HB4HB/RS (90/10/7 untreated)	1.6 ± 0.5	20.2 ± 1.2	1.4 ± 0.3	9.0 ± 0.5
PLA/P3HB4HB/RS (90/10/3 treated)	1.4 ± 0.1	30.9 ± 3.1	2.7 ± 0.4	26.1 ± 1.2

Chapter 5

Conclusions

PLA/P3HB4HB blends and PLA/P3HB4HB composite films were successfully prepared through compression molding, and the influence of incorporating rice straw (RS) was explored in terms of morphological, thermal, gas barrier, and mechanical properties.

In the PLA/P3HB4HB blend films, an increase in P3HB4HB content from 20 to 40 wt% resulted in the increasing size of P3HB4HB domains, indicating heterogeneous phases in immiscible blends. The higher melting temperature of both polymers was attributed to the bulky and large size of P3HB4HB domain, potentially restricting polymer mobility and leading to reduced crystallinity percentages (X_c). The immiscible blend suggested weak interfacial adhesion between the polymer phases, allowing the flow of oxygen gas and water vapor throughout the films. Additionally, a decrease in mechanical properties observed in most blends, excepting, in the case of the PLA/P3HB4HB blend (90/10), exhibited synergistic behavior in toughness.

In PLA/P3HB4HB composite films, the addition of untreated RS fiber (3 to 7 phr) revealed gaps between the RS fiber and polymer matrix, indicating weak interfacial adhesion and contributing to increased oxygen and water vapor transmission rates (OTR and WVTR). However, the influence of hydroxyl groups in RS fiber dominated over the gaps, resulting in a decrease in WVTR values, indicating an enhancement in the barrier properties of RS fiber. Untreated RS fiber also caused a reduction in the X_c , as evident from DSC and POM analyses. Conversely, alkali treatment eliminating lignin species enhanced the X_c of the composite filled treated RS. Additionally, untreated RS fiber increased young's modulus, reducing the flexibility of the composites. However, the addition of 7 phr untreated RS fiber led to fiber agglomeration, resulting in decreased mechanical properties. Finally, it can be seen that the alkaline treatment of RS fiber is evident in its enhanced nucleating agent efficiency and improved ability to establish stronger interfacial adhesion between RS fiber and polymer matrix. This enhancement in interfacial adhesion contributes to improved effectively blocking the oxygen and water vapor flow, and the flexibility in the composites.

REFERENCES

1. Arrieta, M.P., et al., *Ternary PLA-PHB-Limonene blends intended for biodegradable food packaging applications*. European Polymer Journal, 2014. **50**: p. 255-270.
2. Idris Zembouai, S.B., Mustapha Kaci, Aida Benhamida, Yves-Marie Corre, Yves Grohens, Aurélie Taguet & José-Marie Lopez-Cuesta *Poly(3-Hydroxybutyrate-co-3-Hydroxyvalerate)/Polylactide Blends: Thermal Stability, Flammability and Thermo-Mechanical Behavior*. Journal of Polymers and the Environment, 2013. **22**(1): p. 131-139.
3. Aversa, C., M. Barletta, and N. Koca, *Processing PLA/P(3HB)(4HB) blends for the manufacture of highly transparent, gas barrier and fully bio-based films for compostable packaging applications*. Journal of Applied Polymer Science, 2023. **140**(13).
4. Che, X.-M., H.-M. Ye, and G.-Q. Chen, *Effects of uracil on crystallization and rheological property of poly(R-3-hydroxybutyrate-co-4-hydroxybutyrate)*. Composites Part A: Applied Science and Manufacturing, 2018. **109**: p. 141-150.
5. Potdar, P.P., et al., *Valorization of paddy straw through development of PLA-paddy straw fibre reinforced composites and their physical, morphological, mechanical and thermal characterization*. Biomass Conversion and Biorefinery, 2023.
6. Niu, D., et al., *Enhanced crystallization, heat resistance and transparency of poly(lactic acid) with self-assembling bis-amide nucleator*. Int J Biol Macromol, 2023. **234**: p. 123584.
7. Chen, Z., et al., *Novel bioresource-based poly(3-Hydroxybutyrate-co-4-Hydroxybutyrate)/poly(LacticAcid) blend fibers with high strength and toughness via melt-spinning*. Journal of Applied Polymer Science, 2020. **137**(32).
8. Sari, F.P. and B. Budiyo, *Enhanced biogas production from rice straw with various pretreatment : a review*. Waste Technology, 2014. **2**(1).
9. Singh, S., et al., *Rice Straw Based Natural Fiber Reinforced Polymer for*

- Sustainable Bio- Composites: A Systematic Review*. Evergreen, 2023. **10**(2): p. 1041-1052.
10. Singh, H. and A. Chatterjee, *Lignocellulosic biowaste for composite applications, in Functional and Technical Textiles*. 2023. p. 639-678.
 11. Yang, Q., et al., *Effect of Chemical Treatment on Rice Straw Fiber Surface and Properties of Straw/Polylactic Acid Composites*. *Journal of Natural Fibers*, 2023. **20**(2).
 12. Zembouai, I., et al., *A study of morphological, thermal, rheological and barrier properties of Poly(3-hydroxybutyrate-Co-3-Hydroxyvalerate)/polylactide blends prepared by melt mixing*. *Polymer Testing*, 2013. **32**(5): p. 842-851.
 13. Homklin, R. and N. Hongsriphan, *Mechanical and Thermal Properties of PLA/PBS Co-continuous Blends Adding Nucleating Agent*. *Energy Procedia*, 2013. **34**: p. 871-879.
 14. Luo, R., K. Xu, and G.-Q. Chen, *Study of miscibility, crystallization, mechanical properties, and thermal stability of blends of poly(3-hydroxybutyrate) and poly(3-hydroxybutyrate-co-4-hydroxybutyrate)*. *Journal of Applied Polymer Science*, 2007. **105**(6): p. 3402-3408.
 15. Pongputthipat, W., Y. Ruksakulpiwat, and P. Chumsamrong, *Development of biodegradable biocomposite films from poly(lactic acid), natural rubber and rice straw*. *Polymer Bulletin*, 2022. **80**(9): p. 10289-10307.
 16. Lendvai, L., *Lignocellulosic agro-residue/poly(lactic acid) (PLA) biocomposites: Rapeseed straw as a sustainable filler*. *Cleaner Materials*, 2023. **9**.
 17. Poornejad, N., K. Karimi, and T. Behzad, *Improvement of saccharification and ethanol production from rice straw by NMMO and [BMIM][OAc] pretreatments*. *Industrial Crops and Products*, 2013. **41**: p. 408-413.
 18. Thulluri, C., R. Balasubramaniam, and H.R. Velankar, *Generation of highly amenable cellulose-Ibeta via selective delignification of rice straw using a reusable cyclic ether-assisted deep eutectic solvent system*. *Sci Rep*, 2021. **11**(1): p. 1591.
 19. Moneim, M.A., et al., *Direct conversion of an agricultural solid waste to hydrocarbon gases via the pyrolysis technique*. *Egyptian Journal of Petroleum*,

2018. **27**(4): p. 991-995.
20. Chirayil, C.J., et al., *Isolation and characterization of cellulose nanofibrils from Helicteres isora plant*. Industrial Crops and Products, 2014. **59**: p. 27-34.
 21. Dilamian, M. and B. Noroozi, *A combined homogenization-high intensity ultrasonication process for individualizaion of cellulose micro-nano fibers from rice straw*. Cellulose, 2019. **26**(10): p. 5831-5849.
 22. Sakhiya, A.K., et al., *Thermal decomposition of rice straw from rice basin of India to improve energy-pollution nexus: Kinetic modeling and thermodynamic analysis*. Energy Nexus, 2021. **4**.
 23. Arup R, B., Anup K. Ghosh, Ashok Misra., *Reactively compatibilised polymer blends: a case study on PA6/EVA blend system*. Polymer, 2001.
 24. Molavi, F.K., et al., *Design and Characterization of Novel Potentially Biodegradable Triple-Shape Memory Polymers Based on Immiscible Poly(l-lactide)/Poly(ϵ -caprolactone) Blends*. Journal of Polymers and the Environment, 2019. **27**(3): p. 632-642.
 25. Kantesh Balani, V.V., Arvind Agarwal, Roger Narayan., *Physical, Thermal, and Mechanical Properties of Polymers*, in *Biosurfaces*. 2014. p. 329-344.
 26. Xie, X.L., et al., *Structural properties and mechanical behavior of injection molded composites of polypropylene and sisal fiber*. Polymer Composites, 2004. **23**(3): p. 319-328.
 27. Davachi, S.M., et al., *Investigating the Effect of Treated Rice Straw in PLLA/Starch Composite: Mechanical, Thermal, Rheological, and Morphological Study*. Advances in Polymer Technology, 2015. **37**(1): p. 5-16.
 28. Sebastian Tamayo-Vegas, A.M., Chang Liu, Mostapha Tarfaoui, and Khalid Lafdi., *The Effect of Agglomeration on the Electrical and Mechanical Properties of Polymer Matrix Nanocomposites Reinforced with Carbon Nanotubes*. Polymer, 2022.
 29. Tamayo-Vegas, S., et al., *The Effect of Agglomeration on the Electrical and Mechanical Properties of Polymer Matrix Nanocomposites Reinforced with Carbon Nanotubes*. Polymers (Basel), 2022. **14**(9).



จุฬาลงกรณ์มหาวิทยาลัย
CHULALONGKORN UNIVERSITY

VITA

NAME Danaipat Tuangwattanasin
DATE OF BIRTH 11 October 1997
PLACE OF BIRTH Suratthani, Thailand
INSTITUTIONS ATTENDED Engineering Kasetsart University, Bangkok, Thailand
HOME ADDRESS 21, Moo3, Huai Phra, Don Tum, Nakhon Pathom 73150

